Microfluidic Handling of DNA for Spatial Genome Research

2022 CNF REU Intern: Eryka Kairo

Intern Affiliation: Physics Department, Seton Hall University

CNF REU Principal Investigator: Dr. Warren Zipfel, Meinig School of Biomedical Engineering, Cornell
CNF REU Mentor: Jack Crowley, Meinig School of Biomedical Engineering, Cornell University
CNF REU Project and Primary Source(s) of Research Funding: 2022 Cornell NanoScale Science & Technology Facility Research Experiences for Undergraduates (CNF REU) Program via the National Science Foundation under Grant No. NNCI-2025233
Contact: eryka.kairo@gmail.com, wrz2@cornell.edu, jcc453@cornell.edu
Website: https://cnf.cornell.edu/education/reu/2022
Primary CNF Tools Used: ABM Contact Aligner, Class II Photoresist Room, P7 Profilometer

Abstract:

Nuclear envelope invaginations that contain endoplasmic reticulum (ER), mitochondria and other cytosolic organelles have been linked to cancer, and can be used as tumor biomarkers. To gain a better understanding of how this occurs, the organization and composition of chromatin near nuclear invaginations needs to be examined. Assuming that these invaginations are involved in cell signaling and transcription, they may control disease-specific phenotypes through spatial gene regulation.

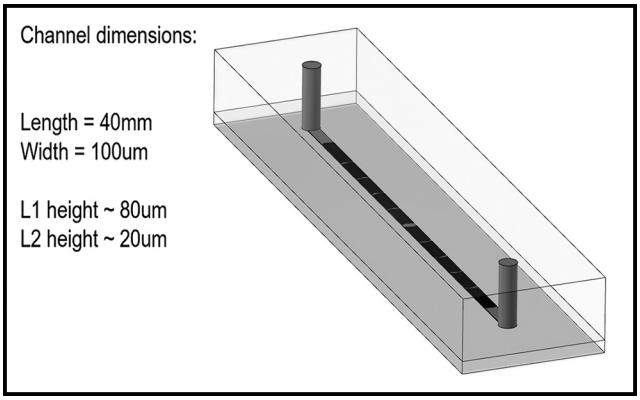

Figure 1: Schematic design of microfluidic device.

To explore spatial control of gene regulation, we have developed a method that enables chromatin isolation from small (femtoliter scale) targeted volumes within the nucleus. The method, we call Femto-seq, uses localized nonlinear excitation to photo-biotinylate small nuclear volumes so that chromatin can be obtained using affinity purification, and then sequenced. To improve the throughput and efficacy of Femto-seq, here we demonstrate a microfluidic purification device utilizing a single fluidic channel with a functionalized surface and mixing elements that improve sample yield and the level of purification. When validated and employed, our microfluidic devices will enhance the capacity of Femto-seq to elucidate spatial gene regulation patterns associated with nuclear invaginations.

The device was fabricated using multilayer SU-8 photolithography. Herringbone structures were added along the fluidic channel to encourage "chaos" in flow patterns of our sample through the channel, increasing the capture efficiency and improve our purification yield. We utilized a negative resist and our design was cast into PDMS and bonded to a glass surface. Our device was characterized through fluorescence microscopy and biochemical assays to first, validate that a streptavidin-biotin complex is formed using a glass functionalization protocol, and then to optimize an elution protocol suitable for our device and quantify our yield and purity of biotinylated deoxyribonucleic acid (DNA).

Summary of Research:

Our project goal for this summer was to fabricate and optimize a microfluidic device that can immobilize biotinylated DNA. The device design was already determined by mentor Jack Crowley, which was a single fluidic channel that had added mixing elements called herringbones on the top of the channel, both embedded in a layer of polydimethylsiloxane (PDMS) as shown in Figure 1.

The PDMS is then binded onto a glass slide to close the channel. To achieve this goal, the project had three main parts. The first part was the wafer fabrication and the device construction, and our methodology for this part was to use multi-layer SU-8 soft photolithography because the design required the fluidic channel to be treated as one layer during photolithography, and the herringbones to be treated as another; the second part was to functionalize the device surface in order to immobilize streptavidin on to the glass substrate and take advantage of the very strong affinity between streptavidin and biotin; the final part was validation and characterization of the device, and to set up an engineering system to optimally operate the device.

The first portion of the project took the longest because we were in unfamiliar territory working with multi-layer photolithography — so there was a lot of trial and error. Issues arose when we weren't able to achieve proper contact between our silicon wafer and our photomasks, but by talking to Aaron Windsor and Chris Alpha from the CNF staff, we were able to gather some tips and tweak our fabrication process, which yielded better results.

Upon being able to consistently acquire usable channels from this process we were able to move on to the functionalizing portion of the project. This portion involved functionalizing fully constructed devices and validating the protocol worked as intended.

To do this we used fluorescent microscopy and flowed fluorescent biotin through functionalized devices, to image and search for bright sports which correlate to immobilzed biotin. We were able to see that we were immobilizing some biotin, so the next step was to set up an experiment to characterize our device. We chose to use DNA gel electrophoresis to do this as we are able to quantify the DNA bands in the agarose gel after the process, so we would be able to get quantitive data.

We set up the experiment by using DNA gel extraction on a DNA ladder to biotinylate a single length of DNA, and then flowing the ladder and the biotinylated DNA through our device and collecting the flow through. The flow through was run through the gel alongside some baseline samples to learn as much as we could about our device.

Conclusions and Final Steps:

Our next steps begin with completing an engineering system to operate the microfluidic chip. This includes setting up a system that adds an oscillatory washing step within the fluidic channel to increase our purification yield, and would also include adding washing and buffer steps. After this system has been set up, a DNA gel electrophoresis experiment can be run on the device flow-through to validate that biotinylated DNA can be captured using our microfluidic device design and the surface functionalization protocol used works as expected.

Once these have been validated the next step would be to quantify the devices performance, and compare the amount of cells needed to provide a sufficient DNA sample via Femto-seq, and determine the reduction of cells needed for this process from the beginning of the summer, which was 30,000 cells, to now. Next, elution steps to break the strepatavidin-biotin complex formed in this device should be tested and optimized.

The goal is to find a protocol that does minimal damage to the device itself to encourage longevity of the materials used. Part of this elution step would be to develop a flow-through collection protocol that leads to minimal loss of the DNA we worked so hard to affinity capture in the channel. Furthermore, ideally after the steps to optimize this device's function have been established, the system to control the device itself should become programmable, to make device operation as automatic as possible.

References:

[1] Ma, S., et al. 2018. Sci. Adv. 4(4).

[2] Stroock, A.D., et al. 2002. Science 295, 647-51.

A Nanotool for Phase Equilibrium and Water Potential Measurements in Living and Synthetic Systems

CNF Project Number: 1119-03

Principal Investigator(s): Abraham D. Stroock

User(s): Piyush Jain

Affiliation(s): Chemical Engineering, Cornell University

Primary Source(s) of Research Funding: National Science Foundation
Science and Technology Centers (STC);
Air Force Office of Scientific Research

Contact: abe.stroock@cornell.edu, pj248@cornell.edu

Primary CNF Tools Used: Zeta-Sizer

Abstract:

The multiphases water transport in unsaturated porous media has been investigated for a long period yet remains unknown fundamental questions for exploration. In this report, our group developed a nanotool, AquaDust, to measure the local water potential in both living and synthetic unsaturated porous media. In leaves, the disequilibrium in water potential between symplast and apoplast points out a large hydraulic resistance at the plasma membrane of mesophyll cells. In synthetic porous media, a water potential distribution of the wetting front in an imbibition process can enhance the understanding of the capillary properties and the dynamic of the process.

Summary of Research:

The mesophyll in leaves operates as an unsaturated porous medium, with vapor-filled spaces interspersed within a matrix that is wetted by the condensed liquid phase. The undersaturated state introduced a local coupling between phase equilibrium and transport processes in the two phases, and resulted in the strong global coupling of heat and mass transfer. The physic and mathematical model developed by Rockwell et al. shows the competition between these two phases in mesophyll through modeling in Figure 1 [1]. This model strengthened the understanding of the fundamental questions in transport processes, and open a new route for the experimental exploration in both living and synthetic systems.

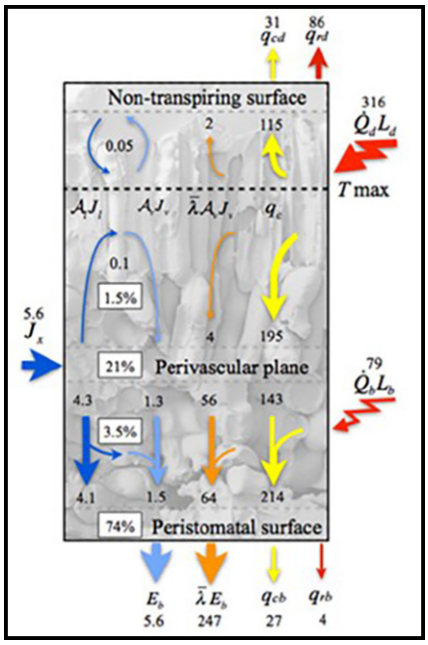

Figure 1: Model prediction of heat and mass flux within a transpiring leaf [1].

In a previous study by our group, a new hydrogel nanoreporter, AquaDust, was developed to report local water potential (Ψ) for *in planta* measurements [2]. Figure 2a shows the mechanism that the gel matrix responds to water potential by shrinking and swelling under dry and wet environments, respectively. The volumetric changes of the matrix will lead to the distance changes between donor and acceptor dyes. Accordingly, the emission spectrum via Förster Resonance Energy Transfer (FRET) between donor and acceptor dyes provides quantitative measurement of water potential in Figure 2b.

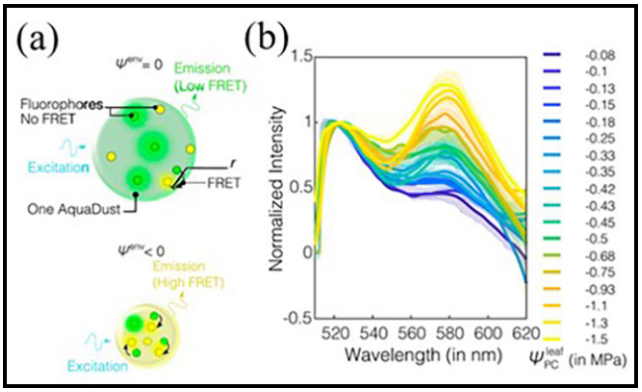

Figure 2: (a) Mechanism of AquaDust responses under wet and dry environments. (b) Spectra of AquaDust in maize leaves at different water potentials. (Jain, et al., 2021.)

The *in planta* measurement of AquaDust provided local water potential in mesophyll. The gradient in water potential of through-thickness section of a maize leaf are depicted in Figure 3a. The inset highlights the disequilibrium in water potential between the symplast

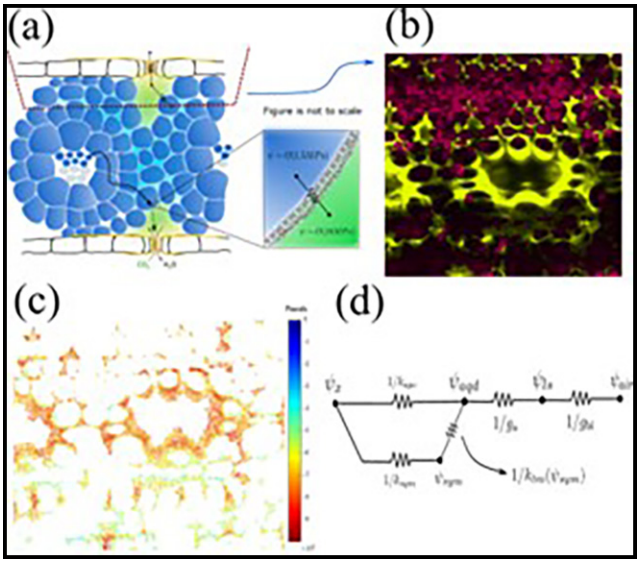

Figure 3: (a) Through-thickness section of a maize leaf depicting the gradient in water potential from xylem to stomates. (b) Confocal microscope image of a horizontal section in a maize leaf. (c) Spatial distribution water potential for the location shown in (b). (d) A model of hydraulic resistances in a maize leaf.

and apoplast. In Figure 3b, the confocal image shows turgid mesophyll cells, with chloroplasts (pink) pushing against cell boundaries (in turgid state), having their cell walls coated with AquaDust (yellow). In Figure 3c, the AquaDust response shows that water potentials in the vapor phase as low as -9 MPa are observed adjacent to turgid cells.

To explain this disequilibrium, we invoke a large hydraulic resistance at the plasma membrane of mesophyll cells, and a model of hydraulic resistances in a maize leaf is shown in Figure 3d. The xylem (Ψ_x) and AquaDust/mesophyll-apoplast (Ψ_{AQD}) nodes are connected by an apoplasmic resistance ($1/k_{apo}$) in parallel with a transmembrane resistance ($1/k_{tm}(\Psi_{sym})$), with the latter assumed to be a variable function of the symplastic water potential; this 'outside-xylem' part of the network is in series with the stomatal resistance ($1/g_s$) and boundary-layer resistance ($1/g_{bl}$).

In the synthetic system, we developed an experimental method to measure water potential distribution in synthetic porous media. First, the relationship between relative FRET efficiency and water potential in Figure 4a was built through measuring relative FRET efficiency under control relative humidity. The relative humidities were converted into water potentials through Kelvin equation [3] and the results were anastomotic with the theory presented in Jain, et al. [2].

Then, an imbibition process was performed in an AquaDust-filled cellulose acetate filter paper to investigate water potential distribution in capillary-driven process. The results before and after imbibition are shown in Figure 4b-c. Within the imbibition area, lower relative FRET efficiency and transition area of wetting front are observed. The detailed water potential

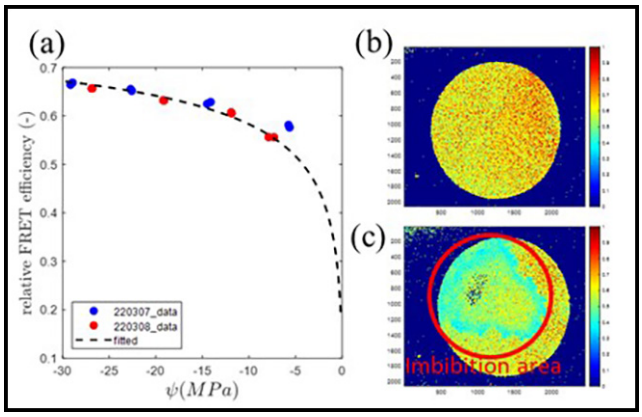

Figure 4: (a) The relative FRET efficiency to water potential data. Dashed line is the theoretical prediction as obtained from the Flory–Rehner theory and dipole-plane FRET model presented in Jain, et al., 2021. (b-c) The relative FRET efficiency (b) before and (c) after imbibition.

distribution in synthetic porous media can enable investigations on capillary properties and dynamic processes.

Conclusions and Next Steps:

AquaDust can provide an outstanding and reliable tool to measure water potential in both living and synthetic systems. For living system, water potential measured by AquaDust shows the disequilibrium in water potential between the symplast and apoplast, indicating a large hydraulic resistance at the plasma membrane of mesophyll cells. In synthetic system, the transition area of water potential in an imbibition process can be clearly recorded by AquaDust.

The next steps of *in planta* experiments presented in Figure 3 should include understanding the molecular mechanism regulating outside-xylem hydraulic conductance (K_{ox}) using tools from genetics such as aquaporin mutants, transcriptomic analysis and treatments using abscisic acid (ABA) and blue light responses [4]. The next steps of synthetic system will be to investigate the coupled heat and mass transport in the thermally loaded unsaturated porous medium by measuring the spatiotemporal water potential.

References:

[1] Rockwell, F.E., N.M. Holbrook, and A.D. Stroock, The competition between liquid and vapor transport in transpiring leaves. Plant Physiol, 2014. 164(4): p. 1741-58.

[2] Jain, P., et al., A minimally disruptive method for measuring water potential in planta using hydrogel nanoreporters. Proc Natl Acad Sci U S A, 2021. 118(23).

[3] Skinner, L. and J. Sambles, The Kelvin equation—a review. Journal of Aerosol Science, 1972. 3(3): p. 199-210.

[4] Shatil-Cohen, A., Z. Attia, and M. Moshelion, Bundle-sheath cell regulation of xylem-mesophyll water transport via aquaporins under drought stress: a target of xylem-borne ABA? The Plant Journal, 2011. 67(1): p. 72-80.

Development of a Biomembrane Platform for the Study of Virus Infection

CNF Project Number: 1686-08
Principal Investigator(s): Susan Daniel
User(s): Zhongmou Chao

Affiliation(s): Smith School of Chemical and Biomolecular Engineering, Cornell University
Primary Source(s) of Research Funding: Defense Threat Reduction Agency
Contact: sd386@cornell.edu, zc83@cornell.edu
Primary CNF Tools Used: Heidelberg Mask Writer - DWL2000, ABM Contact Aligner, Odd-Hour E-beam Evaporator, Oxford PECVD, PT 740 Etcher, DISCO Dicing Saw, Bruker AFM

Abstract:

As a "label-free" alternative to optical sensing, electrical sensing represents a more feasible, reproducible, and scalable detection method [1,2]. Among various electrical sensing techniques, the non-invasive electrochemical impedance spectroscopy (EIS) technique is especially suitable for accurately quantifying the bio-recognition events occurring at a variety of biointerfaces, such as bacterial, viral, cellular and synthetic lipid membranes [3,4]. Our group aims to design a microelectrode system that will support the self-assemble of supported lipid bilayers (SLBs) on the electrode surfaces, and their electrical properties (resistance, capacitance) can be extracted by applying an alternating voltage and recording the current response [4-7]. Since the electrode dimensions and the local environment are readily controlled via photolithography, this system gives us a edge to easily mimic and manipulate the local environment to support the assembly of various SLBs of interest. Future work will focus on the incorporation of the microfluidic system into the microelectrode system.

Summary of Research:

To fabricate the microelectrode devices, photomasks were created using the Heidelberg Mask Writer - DWL2000, and used with the ABM contact aligner to pattern photoresist that was spun onto a fused silica wafer. A first layer of gold contact pad was patterned following the developing of SPR220 3.0 photoresist and the deposition of Au thin film. A thin layer of SiO_2 insulating layer is then deposited directly on top of the Au contact pad using Oxford PECVD.

Electrode area was then patterned on SiO_2 following the spin-coating and developing of the second layer of photoresist. PT-740 etched was then used to etch the exposed SiO_2 until Au contact pad has been exposed. A conductive polymer, PEDOT:PSS was then spun over the fused silica wafer followed by the deposition of a germanium (Ge) hard mask (odd-hour evaporator). A third layer of photolithography was performed on a layer of negative photoresist spun on top of Ge, where all resists above Ge at areas outside active electrode surface have been developed.

Unprotected Ge and PEDOT:PSS underneath were then etched using PT-740. Ge on top of active electrode area was then etched in water bath overnight.

Once the microelectrode device was fabricated, a PDMS well was stamped directly on top to create a reservoir for SLB self-assembling and allow EIS measurement.

References:

[1] Berggren, M., and A. Richter-Dahlfors. "Organic bioelectronics." Advanced Materials 19.20 (2007): 3201-3213.

[2] Chalklen, T., Q. Jing, and S. Kar-Narayan. "Biosensors based on mechanical and electrical detection techniques." Sensors 20.19 (2020): 5605.

[3] Magar, H.S., R.Y.A. Hassan, and A.Mulchandani. "Electrochemical Impedance Spectroscopy (EIS): Principles, Construction, and Biosensing Applications." Sensors 21.19 (2021): 6578.

[4] Lisdat, F., and D. Schäfer. "The use of electrochemical impedance spectroscopy for biosensing." Analytical and Bioanalytical Chemistry 391.5 (2008): 1555-1567.

[5] Tang, T., et al. "Functional infectious nanoparticle detector: Finding viruses by detecting their host entry functions using organic bioelectronic devices." ACS Nano 15.11 (2021) 18142-52.

[6] B.E. Naser, et al. "Detection of Ganglioside-Specific Toxin Binding with Biomembrane-Based Bioelectronic Sensors." ACS Applied Bio Materials 4.11 (2021): 7942-7950.

[7] Pappa, A., et al. "Optical and electronic ion channel monitoring from native human membranes." ACS Nano 14.10 (2020): 12538-12545.

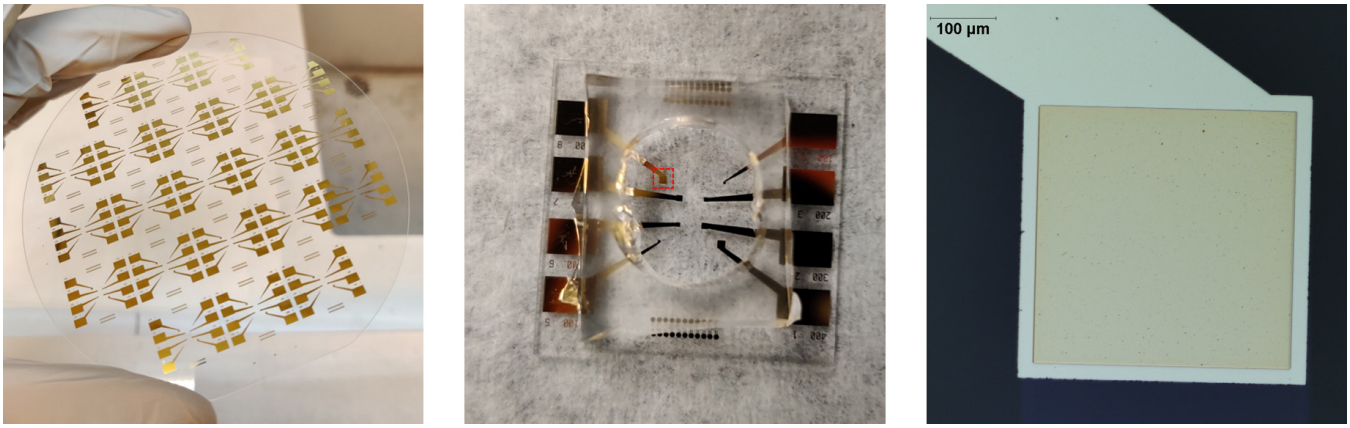

Figure 1: Microelectrode devices on a fused silica wafer (left); PDMS well stamped on a single device to enable self-assembling of SLB and EIS measurement (middle) and zoomed in figure to show PEDOT:PSS electrode on Au contact pad (right).

Resonator Nanophotonic Standing-Wave Array Trap for Single-Molecule Measurements

CNF Project Number: 1738-08

Principal Investigator(s): Michelle D. Wang

User(s): Yifeng Hong

Affiliation(s): a) Department of Electrical and Computer Engineering, Cornell University; b) Department of Physics, Cornell University; c) Howard Hughes Medical Institute

Primary Source(s) of Research Funding: Howard Hughes Medical Institute

Contact: mdw17@cornell.edu, yh874@cornell.edu

Website: http://wanglab.lassp.cornell.edu/

Primary CNF Tools Used: ASML Deep Ultraviolet Stepper, Oxford 100 Plasma Etcher, Oxford 81 Etcher, Oxford 82 Etcher, Unaxis 770 Deep Si Etcher, Heidelberg Mask Writer - DWL2000, SÜSS MA6-BA6 Contact Aligner, Gamma Automatic Coat-Develop Tool, LPCVD Nitride - B4 furnace, Wet/Dry Oxide - B2 furnace, AJA Sputter Deposition, Oxford PECVD, SC4500 Odd-Hour Evaporator, SC4500 Even-Hour Evaporator, Zeiss Supra SEM, Zeiss Ultra SEM

Abstract:

Optical trapping force has been the greatest limitation of the nanophototic tweezer platform. To overcome this obstacle, we designed and fabricated a resonator nanophotonic standing-wave trap (RnSWAT) device that supports significant force enhancement. As a result, the maximum force is no longer a limiting factor for standard single-molecule experiments, such as DNA stretching and unzipping. We experimentally demonstrated bound protein localization through unzipping a DNA molecule on the RnSWAT and achieved a maximum trapping force of 20 pN with sub-pN and sub-nm resolution. The RnSWAT is the first reported nanophotonic platform realizing standard table top single-molecule measurements.

Summary of Research:

Our lab developed the nanophotonic standing-wave array trap (nSWAT) device. The nSWAT makes use of two counter-propagating modes to form multiple trapping spots along waveguides [1-7]. The first demonstration of the nSWAT device used a silicon (Si) waveguide (Figure 1) [1]. However, due to the strong non-linear absorption, the laser power cannot be efficiently delivered to the Si waveguide at the trapping region.

To resolve this problem, we developed an Si_3N_4 device coupled with 1064 nm laser for the second generation of the nSWAT (Figure 1) [2]. To generate more force, we designed the waveguide path so that the force would be doubled at the trapping region, which we termed as the double-force nSWAT (Figure 1) [3]. However, these nSWAT devices still could not achieve sufficient force for high-force single-molecule experiments, which typically require at least 15 pN.

Last year, our lab finalized the latest generation of nSWAT. We can now generate ~ 20 pN force using a resonator waveguide loop (Figure 1) [7]. The resonator nSWAT wavegudies were patterned with deep ultraviolet

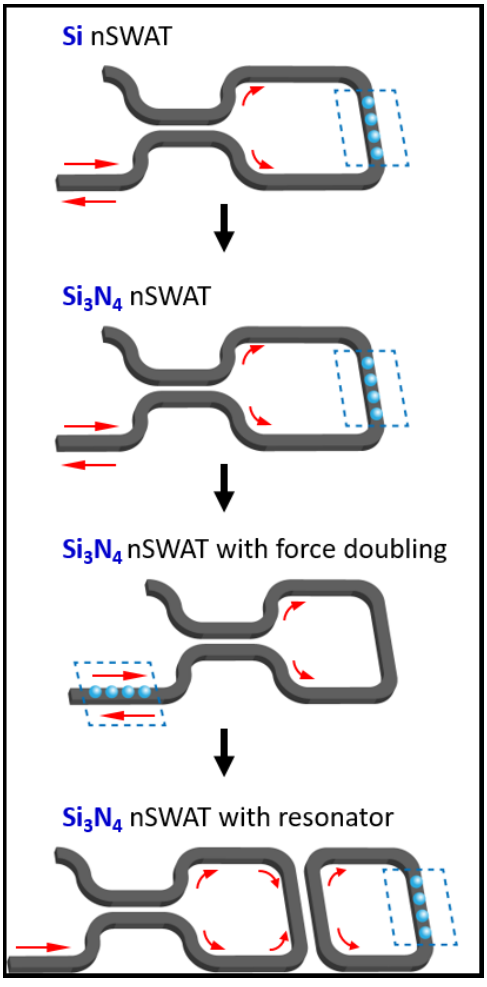

Figure 1: Development progression of the nSWAT platform. Gray structures denote waveguides, and red arrows indicate light propagation [7].

(DUV) lithography. Multiple heaters were deposited on the waveguides (isolated with SiO_2 protection layers) to realize the control of the standing-wave position as well as the resonance condition.

A 15-μm tall and 100-μm wide SU-8 flow channel was patterned to allow the biological sample injection to the waveguides at the trapping region (Figure 2). The resonator nSWAT was then used for single-molecule measurements.

We demonstrated simultaneous unzipping of five DNA molecules [7]. The capability of unzipping through DNA molecules opened up the opportunity of more advanced single-molecule measurements, such as protein localization. We also demonstrated high-throughput ZraI/dCAS9 localization at base-pair resolution with the DNA unzipping mapper technique on the resonator nSWAT [7]. We believe the resonator nSWAT can be a fundamental platform for a broader range of single-molecule applications.

Figure 2: SEM of the fluid pool containing waveguides of the trapping region. The scattering gratings of the four light intensity samplers from the two resonators are clearly visible. Scale bar is 20 μm [7].

References:

[1] M. Soltani, J. Lin, R. A. Forties, J. T. Inman, S. N. Saraf, R. M. Fulbright, M. Lipson, and M. D. Wang, "Nanophotonic trapping for precise manipulation of biomolecular arrays" Nature Nanotechnology 9(6), 448-452 (2014).

[2] F. Ye, R. P. Badman, J. T. Inman, M. Soltani, J. L. Killian, and M. D. Wang, "Biocompatible and high stiffness nanophotonic trap array for precise and versatile manipulation" Nano Letters 16(10), 6661-6667 (2016).

[3] F. Ye, M. Soltani, J. T. Inman, and M. D. Wang, "Tunable nanophotonic array traps with enhanced force and stability" Optics Express 25 (7) 7907-7918 (2017).

[4] J. E. Baker, R. P. Badman, and M. D. Wang, "Nanophotonic trapping: precise manipulation and measurement of biomolecular arrays" WIREs Nanomed Nanobiotechnol. e1477 (2017).

[5] R. Badman, F. Ye, W. Caravan, and M. D. Wang, "High Trap Stiffness Microcylinders for Nanophotonic Trapping" ACS Appl. Mater. Interfaces 11(28), 25074-25080 (2019).

[6] R. Badman, F. Ye, and M. D. Wang, "Towards biological applications of nanophotonic tweezers", Current Opinion in Chemical Biology, 53, 158-166 (2019).

[7] F. Ye, J. T. Inman, Y. Hong, P. M. Hall, M. D. Wang, Resonator nanophotonic standing-wave array trap for single-molecule manipulation and measurement. Nat. Commun. 13, 77 (2022).

Building Microfluidics Devices to Study Zinc Metal Homeostasis in *E. Coli*

CNF Project Number: 1844-09
Principal Investigator(s): Peng Chen
User(s): Felix Alfonso

Affiliation(s): Department of Chemistry and Chemical Biology, Cornell University
Primary Source(s) of Research Funding: National Institutes of Health, National Institute of General Medical Sciences
Contact: pc252@cornelll.edu, fsa33@cornell.edu
Website: http://chen.chem.cornell.edu/
Primary CNF Tools Used: Heidelberg Mask Writer - DWL2000, SÜSS MA6-BA6 Contact Aligner, Oxford Cobra ICP Etcher, Plasma-Therm Deep Silicon Etcher, P7 Profilometer

Abstract:

Microbial life has evolved a set of molecular tools to import the necessary nutrients for survival from their environment and efflux the excess to avoid toxicity. The aim of this study is to elucidate the role individual bacterial cells play in achieving metal homeostasis at the community level. Hence, we constructed a custom-made microfluidic device for the controlled growth of *Escherichia coli* (*E. coli*) colonies in microchambers. The confinement of the cells is achieved by matching the height of the microchambers with the diameter of the *E. coli* cells. Using molecular biology, *E. coli* strains were constructed with fluorescent protein reporters to quantify the gene expression of the influx and efflux ion channels specific to zinc. The dynamic environmental control in microfluidic devices allows us to probe how the community of bacteria achieves zinc metal homeostasis.

Summary of Research:

Zinc is an essential micronutrient for all living organisms [1]. It plays a vital role in protein folding, catalysis, and gene regulation [2,3]. Zinc deficiency or excess is associated with drastic changes in the gut microbiome, which results in poor health [4,5]. Microbial life has evolved a set of molecular tools to import nutrients from their environment and efflux excess nutrients to avoid toxicity. To regulate the efflux pumps, bacterial cells control the transcription of the protein pumps by using metal-responsive transcription regulators that sense the cellular concentration of metal ions to achieve a state of metal homeostasis.

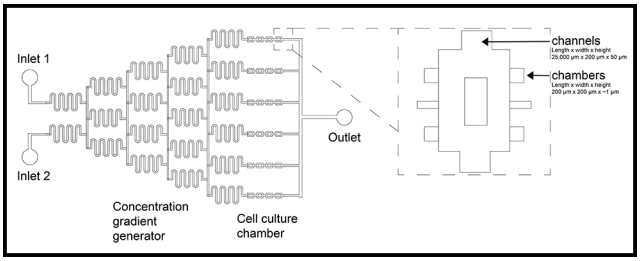

Figure 1: Schematic of the microfluidic device design of the gradient generator, microchannels, and microchambers with the desired dimensions.

The aim of this project is to quantify the management of Zn^{2+} in a microbiome and determine the role individual cells play in achieving metal homeostasis as a community. As a model system, *Escherichia coli* (*E. coli*) will be used to study the community-derived zinc metal regulation. *E. coli* cell's motility and poor adherence to a substrate make it difficult to conduct imaging studies with long time scales. Microfluidics technology is a widely accepted method to study bacterial communities in a controlled environment [6]. A microfluidic platform permits tight control of the nutrients influx and has been successfully used for long-timescale imaging studies [7].

The microfluidic device used in this study consist of three necessary components: a gradient generator, channels, and microchambers (Figure 1). The depth of the microchamber has been chosen to match the diameter of an *E. coli* cell (~1μm) thus facilitating the confinement of the colonies [8]. The microfluidics devices are constructed using well-established silicon nanofabrication technology.

The fabrication scheme is summarized in Figure 2. Briefly, silicon wafers were cleaned with piranha solution from the Hamatech wafer processor. Afterward, they

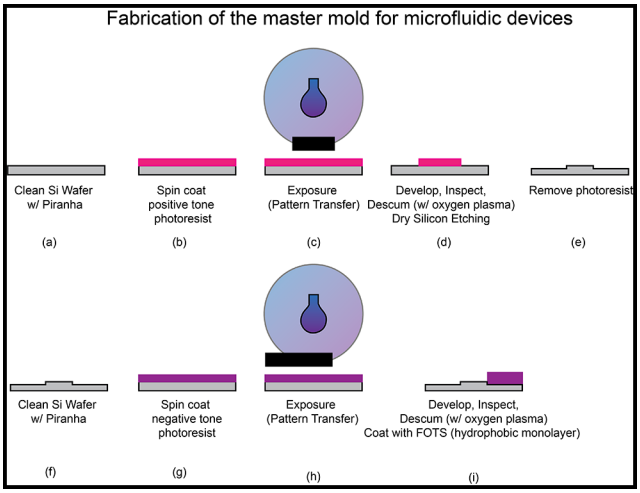

Figure 2: Fabrication of microfluidic devices combining dry etching to construct the chambers and SU-8 lithography to construct the channels.

were spin-coated with photoresists. The photoresist was removed 2 mm from the edge of the wafer using the edge bead removal system. The substrate was patterned using a pre-patterned photomask made using the Heidelberg Mask Writer - DWL2000. The SÜSS MA6-BA6 contact aligner was used for the UV light exposure of the wafer. After developing the wafer and cleaning it with a brief oxygen plasma. The chamber was created by etching about ~ 1 µm of silicon using the Oxford Cobra ICP Etcher. The photoresist was removed using the photoresist stripper bath. The height of the chamber was measured using a profilometer. The channels were constructed using SU-8 lithography.

Briefly, SU-8 was spin-coated onto the substrate and pattern using the SÜSS MA6-BA6 contact aligner. The SU-8 was cured on a hot plate at 95°C. The unpolymerized SU-8 was removed with the developer and the resulting structure was hard baked for 10 minutes at 200°C.

The final step was coating the silicon mold with a hydrophobic molecular monolayer such as tridecafluoro-1,1,2,2-tetrahydrooctyl trichlorosilane (FOTS) to facilitate PDMS removal. After casting PDMS on the silicon mold, the microfluidic devices were bonded to coverslips and inspected using a microscope.

The cells were loaded into the chambers and imaged using a microscope equipped with the appropriate laser line and filters. The composite image shown in Figure 3 shows an example of a chamber loaded with *E. coli*. The cells colored in green are bacterial cells expressing the zinc efflux channels while the cell colored in red indicates the expression of the zinc influx channels.

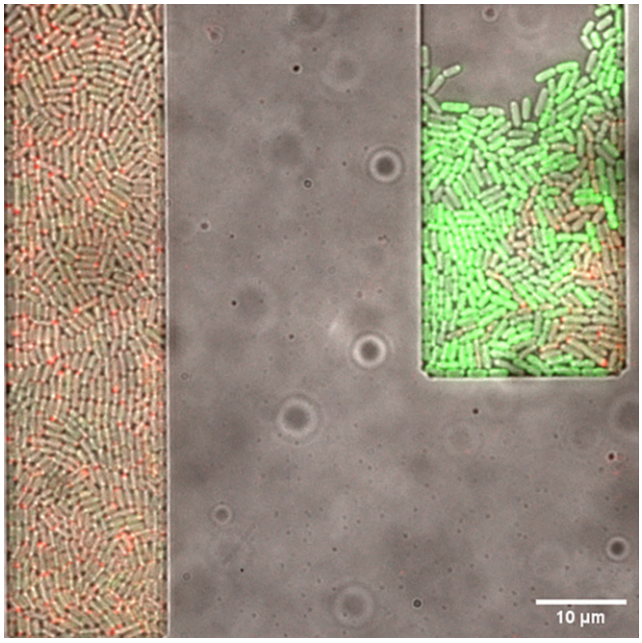

Figure 3: A composite image of E. coli *cells residing in the microchambers expressing influx ion channels (red) and efflux ion channels (green).*

References:

[1] R. R. Robert, B. Saper, Zinc: An Essential Micronutrient. Am. Fam. Physician. 79, 768 (2009).

[2] S. Tan, D. Guschin, A. Davalos, Y.-L. Lee, A. W. Snowden, Y. Jouvenot, H. S. Zhang, K. Howes, A. R. McNamara, A. Lai, C. Ullman, L. Reynolds, M. Moore, M. Isalan, L.-P. Berg, B. Campos, H. Qi, S. K. Spratt, C. C. Case, C. O. Pabo, J. Campisi, P. D. Gregory, Zinc-finger protein-targeted gene regulation: genome wide single-gene specificity. Proc. Natl. Acad. Sci. U. S. A. 100, 11997-12002 (2003).

[3] C. Andreini, I. Bertini, in Encyclopedia of Metalloproteins (Springer, New York, NY, 2013), pp. 2549-2554.

[4] S. R. Gordon, S. Vaishnava, Zinc supplementation modulates T helper 17 cells via its effect on gut microbiome. The Journal of Immunology. 204, 83.18-83.18 (2020).

[5] O. Koren, E. Tako, Chronic Dietary Zinc Deficiency Alters Gut Microbiota Composition and Function. Proc. AMIA Annu. Fall Symp. 61, 16 (2020).

[6] F. Wu, C. Dekker, Nanofabricated structures and microfluidic devices for bacteria: from techniques to biology. Chem. Soc. Rev. 45, 268-280 (2016).

[7] D. Binder, C. Probst, A. Grünberger, F. Hilgers, A. Loeschcke, K.-E. Jaeger, D. Kohlheyer, T. Drepper, Comparative Single-Cell Analysis of Different *E. coli* Expression Systems during Microfluidic Cultivation. PLoS One. 11, e0160711 (2016).

[8] A. Groisman, C. Lobo, H. Cho, J. K. Campbell, Y. S. Dufour, A. M. Stevens, A. Levchenko, A microfluidic chemostat for experiments with bacterial and yeast cells. Nat. Methods. 2, 685-689 (2005).

Biomechanics of Bacteria

CNF Project Number: 1970-10

Principal Investigator(s): Christopher J. Hernandez

User(s): Christine Harper, Junsung Lee, Ellen van Wjingaarden, C.J. Hernandez

Affiliation(s): Sibley School of Mechanical and Aerospace Engineering, Biomedical Engineering Department; Cornell University

Primary Source(s) of Research Funding: NSF 2055214, 2135586, 2125491

Contact: cjh275@cornell.edu, ceh272@cornell.edu, jl3939@cornell.edu, ewv8@cornell.edu

Website: hernandezresearch.com

Primary CNF Tools Used: Deep UV Photolithography, AJA Sputter Deposition, ASML, PT 770, Oxford 100, MOS Clean Anneal

Abstract:

In this project we seek to understand the biomechanical properties of individual bacteria as well as bacterial mechanobiology (the response of living bacteria to mechanical stimuli). We have two goals in this project: 1) to understand how physical forces influence bacterial resistance and tolerance to antibiotics; and 2) to understand how to embed and maintain viable bacteria within rigid materials, the so-called "engineered living material."

Summary of Research:

We have designed microfluidic systems that allow us to apply mechanical loads to individual bacteria and observe the cellular response. We manufacture our devices on silica glass wafers using DUV photolithography to achieve nanoscale features (250 nm smallest dimension, Figure 1). We have demonstrated that mechanical stimuli applied to individual bacteria interrupt the assembly of the tripartite efflux pump responsible for removing copper and silver from the bacteria, CusCBA [1].

We recently demonstrated that mechanical stresses within the bacterial cell envelope also interrupt the function of the MacAB-TolC efflux pump which is used by bacteria remove aminoglycoside antibiotics. Additionally, we have developed mechanical modelling methods that allow us to use the results of our experiments as a measure of the elastic modulus of the bacterial cell envelope [2].

In our most recent work, we have demonstrated that mechanical stress within the cell envelope of the pathogen *Vibrio cholerae* stimulates cell wall repair mechanisms through the VxrAB two-component regulatory system [3].

This finding is exciting in that it suggests that mechanical stress and strain regulate maintenance of the bacterial cell envelope, which is the primary load carrying component of bacteria and the primary target of bacteriocidal antibiotics.

We were recently awarded two grants from the National Science Foundation to explore methods of populating rigid materials with living bacteria and the effects of mechanical stimuli on bacterial biomineralization.

References:

[1] Genova, L.A., Roberts, M.F., Wong, Y-C, Harper, C.E., Santiago, A.G., Fu, B., Srivastava, A., Jung, W., Kreminski, L., Mao, X., Sun, X., Yang, F., Hui, C-Y, Chen, P, Hernandez, C.J.. (2019) "Mechanical Stress Compromises Bacterial Toxin Efflux." Proc Natl Acad Sci U S A. 116 (51) 25462-25467, https://www.pnas.org/content/early/2019/11/25/1909562116.

[2] Lee, J., Harper, C.E., Zhang, W., Ramsukh, M., Bouklas, N., Chen, P., Hernandez, C.J. (2022) "Determining the Young's Modulus of the Bacterial Cell Envelope Using Microfluidic-based Extrusion Loading." Submitted.

[3] Harper, C.E., Zhang, W., Shin, J., van Wjingaarden, E., Chou, E., Lee, J., Wang, Z., Dörr, T., Chen, P., Hernandez, C.J. (2023) "Mechanical stimuli activate gene expression for bacterial cell-wall synthesis." In preparation.

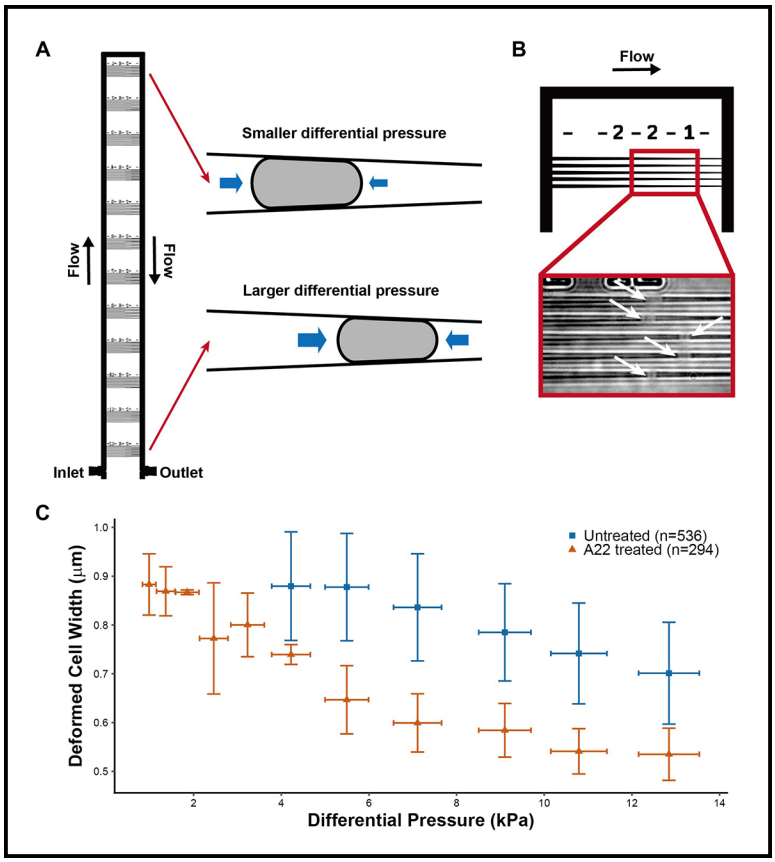

Figure 1: (A) The microfluidic device is shown. Bacteria in liquid media flow through the large bypass channel or become trapped by fluid pressure within the nanoscale tapered channels. The tapered channels are in sets of five, each set providing a different magnitude of differential pressure. (B) E. coli *trapped within the tapered channels are shown. (C) The results of an experiment in which* E. coli *are placed within the device untreated or after treatment with the small molecule A22 that depolymerizes the structural protein MreB, resulting in a less stiff cell as seen from the smaller cell width at each applied differential pressure.*

Design and Application of Microfluidic Devices to Study Cell Migration in Confined Environments

CNF Project Number: 2065-11

Principal Investigator(s): Jan Lammerding

User(s): Richa Agrawal, Maggie Elpers, Julie Heffler

Affiliation(s): Meinig School of Biomedical Engineering, CNF, Weill Institute; Cornell University

Primary Source(s) of Research Funding: National Institutes of Health award R01 HL082792, National Institutes of Health award R01 GM137605, National Institutes of Health award 1U54 CA210184

Contact: jan.lammerding@cornell.edu, ra664@cornell.edu, mae228@cornell.edu, jh2347@cornell.edu

Website: http://lammerding.wicmb.cornell.edu/

Primary CNF Tools Used: PT 770 Deep Silicon Etcher, Oxford Cobra Etcher, Heidelberg Mask Writer - DWL2000, SÜSS MA6 Contact Aligner, Anatech SCE-110-RF Resist Stripper, P-7 Profilometer, MVD 100, SU-8 Lithography Room (Spinners, Hot Plates, etc.)

Abstract:

The ability of cells to migrate through tissues is an essential factor during development, tissue homeostasis, and immune cell mobility. At the same time, it enables cancer cells to invade surrounding tissues and metastasize. We have created microfluidic devices that mimic the narrow, heterogeneous interstitial spaces and that can be used to study nuclear mechanobiology during confined migration. Using these devices in combination with fluorescent imaging, we have developed a method to assess the confined migration fitness of varying cell types.

Research Summary:

During *in vivo* migration, cells such as immune cells, fibroblasts, or metastatic tumor cells traverse interstitial spaces as small as 1-2 μm in diameter. This 'confined migration' requires the deformation not only of the soft cell body but also the rate-limiting step of deforming the large (5-10 μm diameter) and relatively rigid nucleus [1]. To study these processes in more detail, we have previously designed and fabricated polydimethyl siloxane (PDMS) microfluidic devices to model the tight three-dimensional constrictions that metastatic cancer cells may encounter during the metastatic process [2]. These devices support a wide range of cell lines and enable high-quality fluorescence imaging of nuclear lamina bucking, chromatin strain, DNA damage and nuclear rupture/blebbing and repair [2-4]. However, these devices require time-consuming single-cell analysis, do not fully mimic the heterogeneously confining nature of interstitial spaces, and do not allow use of sufficient cell numbers for biological and genomic analyses of cells that have migrated through the confined spaces due to their relatively small constriction areas (Figure 1).

To overcome these limitations, we have designed novel migration devices that mimic the intermittent confinement of interstitial environments using a precisely controlled but heterogeneous "field of pillars" with variable spacing [5] (Figures 1,2). We have created two different geometries of these devices optimized for (1) rapid, easy assessment of migratory fitness as a function of distance traveled, and (2) collection of cells that have successfully completed confined migration through precisely defined constrictions.

One type of device (Figure 2a) features a large constriction area that is compatible with time-lapse microscopy and also enables assessment of migratory fitness from single images captured on multiple consecutive days (Figure 3). Another device design (Figure 2b) features a shorter pillared distance (i.e., fewer constrictions) and is well suited for easy collection of large numbers of cells following confined migration. In ongoing studies, we are combining these devices with the use of the LEGO-optical barcoding system, which utilizes combinations of red, green, and blue fluorescent markers to monitor individual cells based on their distinguishable and heritable colors. This enables us to track cells and their progeny over days and weeks and to quantify the varying abilities of different cells to perform confined migration and to tolerate the associated physical stress. This experimental pipeline presents a high-throughput method for observing the short- and longer-term effects

of mechanically induced nuclear deformation and rupture on cancer cell function and survival.

In order to microfabricate the constriction layer of these designs, we etch silicon using hydrogen bromide in the Oxford Cobra etcher, which has proven to be a highly efficient, reliable method to achieve vertical sidewalls necessary for PDMS devices (Figure 4). We have found this to be advantageous over other etching methods or SU-8 lithography because it provides sufficient resolution of the fine (1 µm) features, and is more reliable and practical than using the photonics etch on the Unaxis 770 and seasoning/re-seasoning the chamber. We continue to use SU-8 photolithography for rapid prototyping and versions of the device which do not require very closely spaced features. Eventually, we will transition this process to a stepper, which will enable us to create "taller" constrictions to serve as a vertically "unconfined control" (>10 µm), which cannot currently be performed using HBr etching. Taken together, these examples illustrate new uses of the available nanofabrication technologies to create improved *in vitro* models to study cancer cell migration.

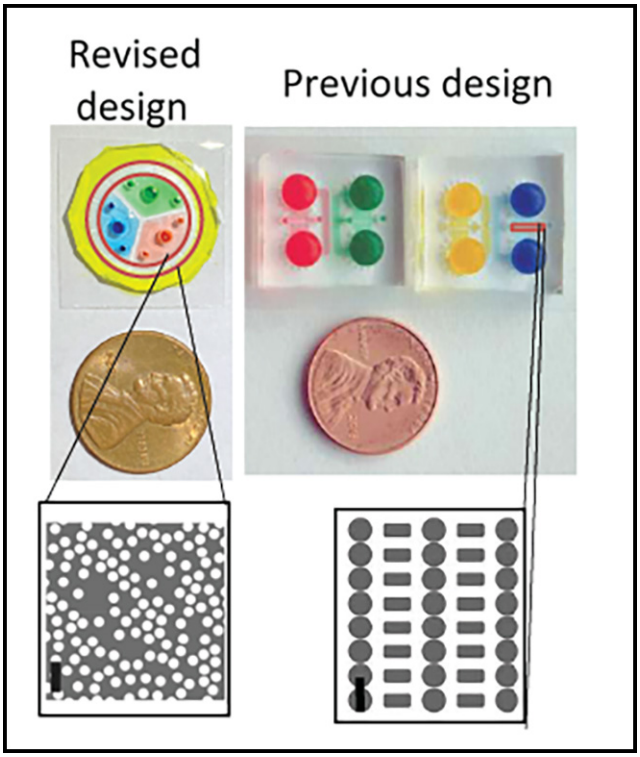

Figure 1: Overview of cancer cell migration device. Top: Partial figure reproduced from Davidson, et al. [2]. Previous PDMS microfluidic devices bonded on glass coverslips and filled with food coloring dye. Bottom: New design of "random pillar" microfluidic devices also bonded to glass coverslip and filled with food coloring. CAD for constriction areas of each design shown (outlined in red on left). Scale bars: 30 µm. All devices have migration areas with 5 µm height. Figure adapted from manuscript submitted to Methods in Molecular Biology.

References:

[1] Davidson, P. M., et al. Nuclear deformability constitutes a rate-limiting step during cell migration in 3-D environments. Cell. Mol. Bioeng. 7, 293-306 (2014).

[2] Davidson, P. M., et al. Design of a microfluidic device to quantify dynamic intra-nuclear deformation during cell migration through confining environments.

[3] Shah, P., et al. Nuclear Deformation Causes DNA Damage by Increasing Replication Stress. Curr. Biol. 31, 753-765.e6 (2021).

[4] Denais, C. M., et al. Nuclear envelope rupture and repair during cancer cell migration. Science (80-.). 352, 353-358 (2016).

[5] Agrawal, R., et al. Assembly and Use of a Microfluidic Device to Study Nuclear Mechanobiology During Confined Migration. Methods Mol Biol. 329-349 (2022).

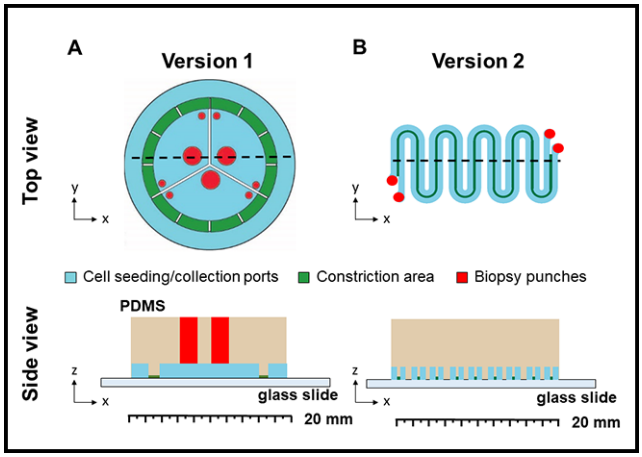

Figure 2: Schematic overview of PDMS migration device geometries. (A) Device optimized for long-term imaging and easy analysis of confined migration efficiency. (B) Device optimized for collection of cells that have completed confined migration. Devices are created by casting PDMS (tan) from wafer and bonded to glass slide to create a confined environment for cancer cell migration (green), after which cells are seeded through biopsy punches (red).

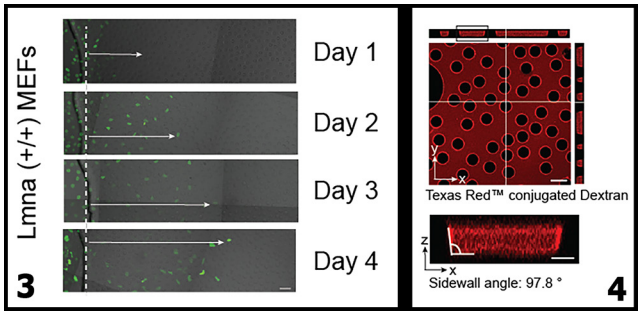

Figure 3, left: Cell migration in microfluidic device. Representative image series to show usage of microfluidic devices to determine migratory fitness as a function of distance traveled from seeding port into constriction area (white arrows) over four days. Figure adapted from manuscript submitted to Methods in Molecular Biology. Figure 4, right: Confocal 3D reconstruction of confined migration area. The PDMS microfluidic device was bonded to a glass coverslip, filled with fluorescent TexasRed-conjugated Dextran, and imaged by confocal microscopy to create a 3D image stacks. Orthogonal projection used to measure sidewall angle, α, of 97.8°. Scale bars: 4 µm. Figure adapted from manuscript submitted to Methods in Molecular Biology.

Development of a 3D Microfluidic Platform for Dynamic Compression of Tumor Spheroids

CNF Project Number: 2068-11

Principal Investigator(s): Dr. Mingming Wu

User(s): Young Joon Suh

Affiliation(s): Department of Biological and Environmental Engineering, Cornell University

Primary Source(s) of Research Funding: NIH Grant R01CA22136, Cornell Center on the Microenvironment and Metastasis (National Center Institute Grant U54CA143876)

Contact: mw272@cornell.edu, ys668@cornell.edu

Website: biofluidics.bee.cornell.edu

Primary CNF Tools Used: Heidelberg Mask Writer – DWL2000, ABM Contact Aligner, P7 Profilometer, MVD100, SUEX Laminator, DISCO Dicing Saw, YES EcoClean Asher, Unaxis 770 Deep Si Etcher, Plasma-Therm Deep Si Etcher, Oxford 81 Etcher, Oxford PECVD, YES Polyimide Oven, Hamatech Hot Piranha

Abstract:

Solid tumor stress caused by rapid growth of tumor cells and abnormality of vascular vessels has long been associated with a poor prognosis of cancer. However, understanding of tumor mechanics has been limited largely to single cells under static compressive loads. In this study, we have developed a high-throughput microfluidic platform providing well-controlled dynamic compression to tumor spheroids.

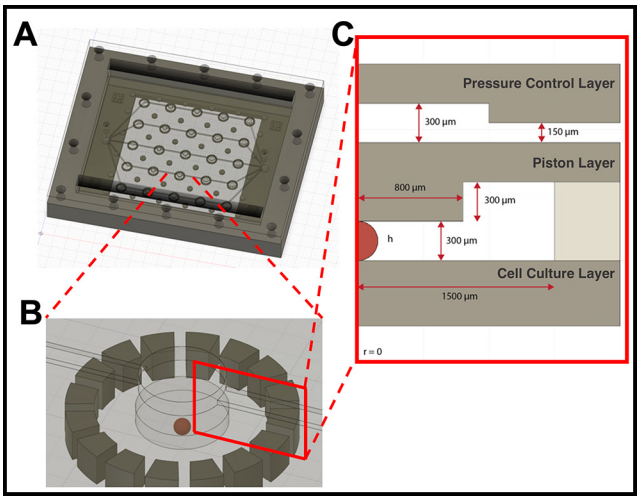

Figure 1: A 3D microfluidic platform for controlled compression of tumor spheroids. (A) An array of 5 × 5 microfluidic compression units. A schematic of an assembled device. Tumor spheroids embedded ECM is loaded into the lower cell culture layer, and pressure regulation media is introduced into the top compression layer. Each column provides five repeats of the same compression magnitude while each row provides five different compression magnitudes. (B) A close-up view of one compression unit. (C) Cross-section view of one compression unit with the dimensions. The PDMS piston is 1600 µm in diameter and the initial distance between the piston and the bottom of the well, h, is 300 µm. The diameters of the five pressure control chambers are 0, 1500, 2000, 2500 to 3000 µm.

Summary of Research:

A 5 × 5 array microfluidic compression device for tumor mechanics studies was designed (see Figure 1). The device consists of three layers: (1) cell culture layer, where the tumor spheroids embedded in extracellular matrices (ECM) are loaded; (2) PDMS piston layer, which is a PDMS membrane that has a top hat shape; and (3) a pressure control layer, which can push the PDMS piston down to apply compressive forces on the tumor spheroids. The three layers are then sandwiched between a Plexiglass® top cover and a stainless-steel frame to provide a good seal. COMSOL modeling has been used to calculate the displacement of the PDMS piston and the force applied on the tumor spheroids at pressure ranging from 0 to 7000 Pa (Figure 2). When pressure is applied in the pressure control chamber, the PDMS piston moves down a distance of Δh, applying a force on the tumor spheroids underneath, and leads to a well-controlled compressive strain, Δh/h, on the spheroids. This device can accommodate tumor spheroids of Young's modulus of about 1250 Pa, that are 100-600 µm in diameter for up to compressive strain (Δh/h) of 0.5.

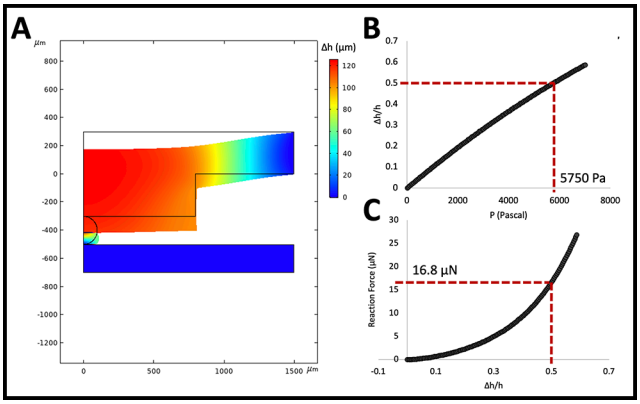

Figure 2: COMSOL computation of a microfluidic compression unit with a tumor spheroid. (A) A colored rendition of COMSOL calculation result of Δh at 7000 Pa of pressure applied. Here, Δh/h = 0.5 at the location of spheroids. The Young's modulus of spheroid and PDMS is 1250 Pa and 2 MPa, respectively. (B) Compressive strain versus applied pressure with spheroid in place. (C) Compression force on spheroid versus compression strain, Δh/h.

Fabrication:

Three layers of the device were fabricated separately. *The cell culture layer* consists of SU-8 wells 600 μm in depth on a 500 μm thick glass (Borofloat®). To fabricate this layer, SU-8 100 was spun on a Borofloat wafer at 475 rpm and soft baked at 95°C for 30 hours. The SU-8 was then exposed to 2310mJ/cm^2 of UV light through a 365 nm filter using an ABM contact aligner. The resist was then post-exposure-baked and developed in the SU-8 developer, followed by a hard bake at 200°C.

The main challenge was to fabricate the height of the wells uniform at 600 μm across the wafer. Keeping the wafer leveled at all steps was found to be crucial.

The piston layer consists of PDMS pistons that are 300 μm in height and 1600 μm in diameter and the PDMS membrane is 300 μm thick. To fabricate the master for this layer, 300 μm wells were etched into a Si wafer. Briefly, 4.5 μm of SPR-220-4.5 was spun on an Si wafer. The resist was then baked at 115°C for 2 mins on a proximity hot plate. Then, it was exposed to the pattern of the pistons at 120 mJ/cm^2 on the ABM contact aligner. After leaving it in room temperature for 30 mins for the post exposure reaction, it was baked at 115°C for 2 mins on a proximity hot plate for the post exposure bake. It was then developed in 726MIF for 120 sec. Then, a mild descum procedure was completed using the Oxford 81 for 90 sec.

Finally, the Si wafer was loaded on the Unaxis 770 Deep Si etcher and a total of 567 loops (200 + 200 + 167) of Bosch process were performed to etch 300 μm into the Si wafer. To remove any excess resist, the wafer was exposed to a strong plasma in a EcoClean Asher. The wafer was then coated with FOTS using the MVD-100 to make the surface hydrophobic. The depth of the piston wells was then measured using the P-7 profilometer.

The pressure control layer is a PDMS membrane with five parallel channels of 200 μm depth. The master is fabricated in a similar way as that for cell culture layer, except that a Si wafer is used instead of a Borofloat wafer.

A 10:1 PDMS was poured and cured on the master molds of the piston and the pressure control layer. After curing the PDMS in a 65°C oven overnight, these two layers were bonded together after plasma treatment and placed in a 90°C oven for 20 mins. Then, these two layers were placed on top of the cell culture layer and sandwiched between a metal frame and a Plexiglass top and connected to a pressure controller.

The compression (Δh) was measured using the defocused particle imaging velocimetry, which was originally developed in our lab [1]. Tumor spheroids were embedded in collagen, which was then introduced into the cell culture chamber. The pressure control chamber is pressurized with a pressure controller. We were able to precisely control the tumor compression with a precision of 1 μm.

References:

[1] Wu, et al., Three-dimensional fluorescent particle tracking at micron-scale using a single camera, Experiments in Fluids, 38, 461 (2005).

Microfabrication of Sample Holders for Cryogenic Small Angle X-Ray Scattering and Flow Cells for Fluorescence Measurements of Ligand Diffusion in Protein Crystals

CNF Project Number: 2157-12

Principal Investigator(s): Robert Thorne

User(s): John Indergaard, Jonathan Clinger, Liam Barnes

Affiliation(s): Laboratory of Atomic and Solid State Physics, Cornell University
Primary Source(s) of Research Funding: National Institutes of Health
Contact: ret6@cornell.edu, jai55@cornell.edu, jac762@cornell.edu, lnb49@cornell.edu
Website: https://www.lassp.cornell.edu/Thorne/
Primary CNF Tools Used: Heidelberg Mask Writer - DWL2000, SÜSS MA6-BA6 Contact Aligner, Oxford 81 / 82 PlasmaLab, VersaLaser Engraver/Cutter, YES Polyimide Curing Oven, SUEX Laminator, Harrick Plasma Generator, Hamatech Wafer Processor, LPCVD CMOS Nitride - E4, Filmetrics Reflectometer, Class II Resist Room

Abstract:

We use microfabrication in our development of methods for probing the structure and dynamics of proteins and other biomolecules. We have fabricated sample cell arrays for high-throughput small-angle X-ray scattering of biomolecules that allow samples to be "immortalized" by cooling to cryogenic temperatures. We are also fabricating crystal trap flow cells for quantitative fluorescence measurements of diffusion coefficients of small molecules inside protein crystals, critical parameters for design and interpretation of time-resolved X-ray crystallography experiments probing enzyme function.

Summary of Research:

CryoSAXS Sample Holders. Small-angle X-ray scattering on biomolecules in solution at room temperature is a workhorse tool for determining biomolecular size, shape, and changes in these due to interactions with other molecules or environmental changes. Our goal is to enable SAXS measurements on samples cooled to (and stored and shipped at) cryogenic temperature. This will allow sample preparation in the home lab as soon as protein is purified, long-term storage, and mail-in, remote data collection at synchrotrons, while dramatically reducing radiation damage and required sample volumes [1].

We have developed and have been evaluating and evolving sample cell arrays for cryoSAXS, shown in Figure 1. The cell arrays consist of pairs of 300 μm thick double-side polished Si pieces, coated on one side with 500 nm of silicon nitride, and KOH-etched to form X-ray transparent nitride windows. Before KOH etching, SUEX sheet is bonded to the nitride-coated side and patterned to form alignment and sealing rings. Thin-wall polyimide tubes are bonded to the rings on one piece, and quartz spacers bonded to fix the X-ray path length through the tubes between windows. X-ray

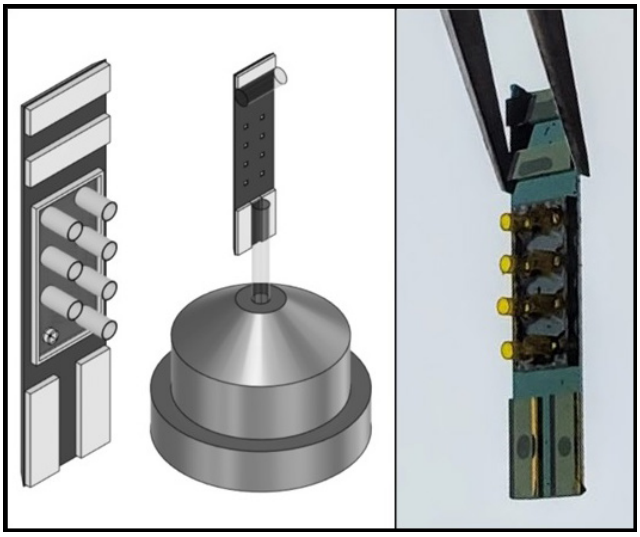

Figure 1: CAD image and photograph of cryoSAXS sample cell arrays. Each sample is held within a polyimide tube between two silicon nitride X-ray windows. The X-ray beam passes axially through the tube. Measurements from two cells in the array, one containing protein+buffer solution and one protein-free buffer solution, must be subtracted to obtain information about the biomolecular structure. As the subtracted diffraction may be 10^{-3} of the total, the cells must be identical.

experiments at CHESS and NSLS-II show that these cells allow rapid cooling of biomolecular samples without ice nucleation and without cracking seen due to differential contraction of sample and cell components (seen in previous cells [2]). However, experiments in the last 18 months identified issues with parasitic upstream X-ray scatter and how this scatter interacts with the sample cells that lead to unacceptable irreproducibility. We are currently addressing this issue, which we believe to be the final major obstacle to obtaining high-quality cryoSAXS data, through changes in cell design and in the experimental configuration at the X-ray beamline. We are also pursuing a simplified, all-microfabricated cell array design in which the polyimide tubes are replaced with high aspect ratio SUEX tubes.

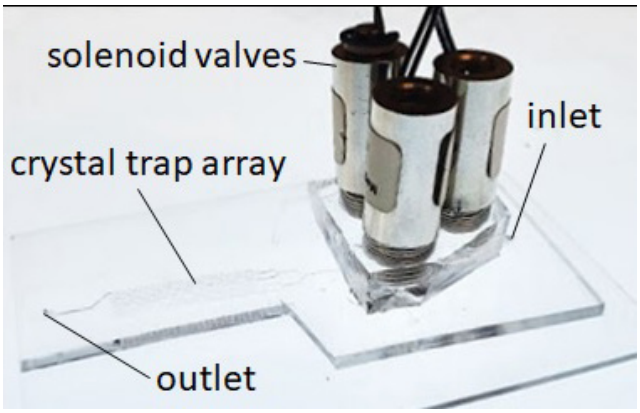

Figure 2: Microcrystal trap array formed by molded PDMS on a glass slide, for measurement of fluorophore diffusion in protein crystals. Solenoid valves control flow of protein crystal-and fluorophore-containing solutions.

Crystal Trap Array Flow Cells. Studying enzymes in action with atomic resolution has been a holy grail in structural enzymology. The most promising methods involve mixing enzyme microcrystals with reactant solution, allowing the reactant to diffuse into the crystal, and then measuring X-ray diffraction at different time delays after mixing [3]. Experiments so far have assumed that diffusion coefficients of reactants in protein crystals are the same as in bulk solution, but theoretical analysis of related problems suggest they may be as much as 10 to 100 times smaller, with major consequences for interpretation of time resolved diffraction experiments.

We are attempting to measure diffusion coefficients of small molecules in protein crystals using either fluorophores or molecules with distinctive intrinsic fluorescence / absorption. To do so, we have fabricated a microcrystal trap array (Figure 2), based on the design and fabrication protocol described in [4]. The traps are loaded by flowing a microcrystal-containing solution through the array. Then a solution containing the small molecule fluorophore is sent through the array, and fluorescence monitored both inside the crystal (using laser scanned microscopy) and in the surrounding solution. The trap array is fabricated from PDMS, and flows are controlled by solenoids.

A master is fabricated by laminating a 100 μm thick SUEX sheet to a silicon wafer, which is then exposed using a mask to define the features of the trap array, and developed. PDMS is poured onto the master with a target thickness of 2 mm, cured, removed, and then bonded to a glass slide. A second, 5 mm thick PDMS layer is then fabricated with screws, centered over the location of input flow channels of the first layer, cast within it. These screws are removed, the second layer bonded to the first, and solenoid valves threaded into the holes. When activated, each solenoid presses down on the first layer of PDMS and collapses the inlet channel over which it is situated.

We successfully tested a valve-free version of the trap array, obtaining fluorescence data from 50 μm crystals and credible diffusion coefficients. The valved version will simplify data collection and improve time resolution.

References:

[1] Meisburger, S. P., et al., (2013) Biophys. J., 104, 227-236.

[2] Hopkins, J. B., et al., (2015) J. Appl. Cryst. 48, 227-237.

[3] Clinger, J. A. et al., (2021). IUCrJ 8, 784-792 (2021).

[4] Lyubimov, A. Y. et al., Acta Cryst. D 71, 928-940 (2015).

Array Microhabitat Platform for Microalgae Growth

CNF Project Number: 2262-13
Principal Investigator(s): Dr. Mingming Wu
User(s): Fangchen Liu

Affiliation(s): Department of Biological and Environmental Engineering, Cornell University
Primary Source(s) of Research Funding: United State Department of Agriculture – National Institute of Food and Agriculture
Contact: mw272@cornell.edu, fl373@cornell.edu
Website: biofluidics.bee.cornell.edu
Primary CNF Tools Used: Heidelberg Mask Writer – DWL2000, ABM Contact Aligner, P10 Profilometer, MVD100, VersaLaser Engraver/Cutter Tool

Abstract:

The occurrence of harmful algal blooms (HABs) is increasing at an alarming rate worldwide, threatening water resources and aquatic ecosystems. Nutrients are known to trigger the onset of HABs and systematic investigation at cellular level is lacking. To study the combination effects of multiple nutrients on microalgae growth in a high throughput way, we built a dual-gradient microhabitat device and a micro-scale light gradient generation platform. Using these platforms, the effect of chemical and physical microenvironment on the growth of model microalgal *Chlamydomonas reinhardtii* was revealed.

Summary of Research:

Harmful algal blooms, or HABs, are serious environmental problems, where a sudden growth of algae or cyanobacteria poses threat to freshwater and marine ecosystems. HABs deteriorate drinking water quality and have huge environmental and economic costs. Nutrient enrichment is believed to be the fundamental cause of HABs, and climate change may further intensity the problem [1]. However, there lacks a quantitative/mechanistic understanding of the roles of environmental factors in the onset of HABs at cellular level. The goal of this project is to investigate the synergistic roles of multiple environmental factors in the growth of cyanobacteria.

Environmental conditions known to affect algae growth include nutrients, mainly nitrogen (N) and phosphorous (P), light intensity and temperature. These conditions are hard to control in nature, and also cannot be quantified in a high throughput way in flasks and chemostats. To address the need for quantitative, systematic, and high-throughput screening of environmental factors, we first developed a high throughput array microhabitat platform, capable of generating stable dual nutrient gradients, and used it for monitoring growth of photosynthetic microbes [2]. The device consists of 64 microhabitats in the form of an 8 × 8 array and each habitat is 100 μm × 100 μm × 100 μm. The microhabitat array is surrounded by two sets of side channels each with the width of 400 μm and height of 200 μm. The device design is shown in Figure 1.

The silicon master was fabricated using two-layer SU-8 negative resist photolithography, and pattern was transferred to a thin agarose membrane later used for cell seeding via soft lithography. Applying this platform, we discovered that nutrients N and P synergistically promoted the growth of *Chlamydomonas reinhardtii* (*C. reinhardtii*) (see Figure 2).

In addition to controlling the chemical environment in the microfluidic device, we developed microscope-based light gradient generation platform, compatible with the array microhabitats, for the investigation of the impact of light intensity on algal growth [3]. The controlled light gradient was generated by modifying the transmitted light path of a commercially available inverted microscope (see Figure 3). A piece of 45 mm half-moon mask, made of optical resin, was fabricated using the CO_2 laser cutter, and customized for a half-dark, half-bright gradient. Light gradient was characterized by grayscale values of bright field images and photosynthetically active radiation (PAR) meter measurements. Growth of algal cells under the controlled light gradient was monitored by fluorescence imaging for five days, and the growth curves and growth rates were obtained (see Figure 4). Results showed that the growth of the microalgae was significantly regulated by the light intensity and a Monod kinetics model fit revealed the half saturation constant of light to be 1.9 $\mu mol \cdot m^{-2} \cdot s^{-1}$ for *C. reinhardtii*.

Our results provided the enabling capability of creating multiple controlled environmental parameters, nutrients and light intensity within one platform, which is suitable for growth studies of all photosynthetic micro-organisms. Future study will move a step further to combine the chemical and physical cues and actively working towards incorporating microbial communities in the HAB-on-a-chip platform.

References:

[1] Paerl, Hans W., et al. Environmental Science and Technology (2018): 5519-5529.

[2] Liu, Fangchen, et al. Lab on a Chip 20.4 (2020): 798-805.

[3] Liu, Fangchen and Larissa Gaul, et al. Lab on a Chip (2022) Advance Article.

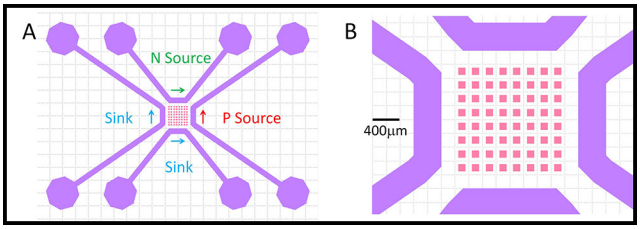

Figure 1: Dual-gradient microfluidic platform design. A. Top view of a device. B. A zoomed-in view of microhabitats and channel. The 8 × 8 array of 100 μm cubic habitats are separated by 100 μm from each other. These habitats are surrounded by four channels with width of 400 μm and height of 200 μm. N source and P source runs through the top and right channel respectively, and the other channels are sink channels. A gradient is generated for each chemical species in the microhabitat array region through molecular diffusion.

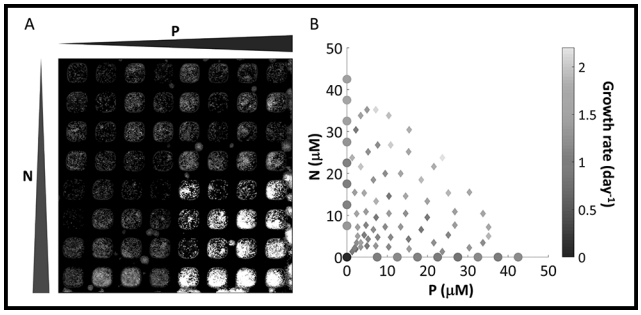

Figure 2: Growth of C. reinhardtii *under nutrients (N, P) gradient. A. Fluorescence images of nutrients co-limited cells growing under N and P dual gradients at day 4. B. The growth rate of* C. reinhardtii *under: control condition, no N or P (dot at the origin), single P gradient (dots on x axis), single N gradient (dots on y axis), and dual-gradient (all the diamonds). Shade is coded for the value of the growth rate.*

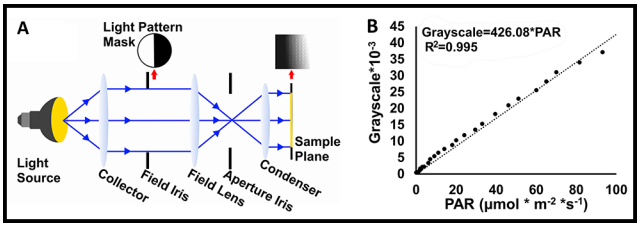

Figure 3: Experimental setup for micrometer-scale light intensity gradient generation and characterization. A. Modifying the light path of a microscope for light gradient generation. Light comes from a halogen lamp. A half-moon light pattern mask was placed directly below the field iris to create the light gradient. Both field and aperture irises were fully open throughout all experiments for optimal, reproducible light gradient generation. (B) Calibration curve of grayscale value from the CCD camera as a function of the light intensity measured by the PAR (photosynthetic active radiation) meter. Dots are the adjusted grayscale values, and the line is a fit to a linear function.

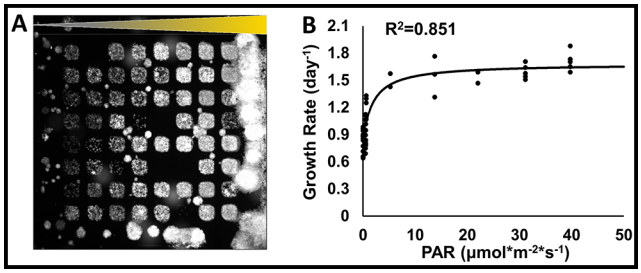

Figure 4: Growth response of C. reinhardtii *to light intensity gradient in an array microhabitat. A. Fluorescence images of cells growing in the array microhabitats under a light intensity gradient at day 5, with approximately 0 PAR on the left side and about 47.7 PAR on the right. B. Growth rate as a function of PAR. Dots are experimental values and line is a fit to Monod model. The fitted coefficients with 95% confidence bounds are μ_0 = 0.823±0.07 day^{-1} μmax' = 0.860±0.099 day^{-1}, and K_s = 1.9±1.18 μmol/(m^2*s), with an R-squared value of 0.851. This data is collected from one of three replicates.*

Metasurface-Enhanced Infrared Spectroscopy for the Measurement of Live Cells

CNF Project Number: 2472-16

Principal Investigator(s): Gennady Shvets

User(s): Steven He Huang, Po-Ting Shen, Aditya Mahalanabish

Affiliation(s): Applied and Engineering Physics, Cornell University

Primary Source(s) of Research Funding: National Cancer Institute of the National Institutes of Health award number R21 CA251052, National Institute of General Medical Sciences of the National Institutes of Health award number R21 GM138947

Contact: gs656@cornell.edu, hh623@cornell.edu, ps944@cornell.edu, am2952@cornell.edu

Website: http://shvets.aep.cornell.edu

Primary CNF Tools Used: JEOL 9500, SC4500 Evaporator, Zeiss Supra SEM, PDMS Casting Station, Anatech Resist Strip, Glen 1000 Resist Strip, Oxford PECVD, Oxford ALD FlexAL, Plasma-Therm 740, DISCO Dicing Saw

Abstract:

We have developed Metasurface-Enhanced Infrared Spectroscopy (MEIRS) as a novel tool to perform spectral analysis of live cells. In MEIRS, cells are cultured on plasmonic nanoantennas (metasurface), which enhances infrared absorption through the plasmonic hotspots. Various cellular responses can be observed from the IR absorption spectra collected in real-time. Our current work focuses on expanding the application of MEIRS through the integration of metasurface with multi-well cell culture chambers for high-throughput measurements, exploring the use of MEIRS to measure cellular response from chemotherapeutics, as well as combining plasmonic metasurfaces with nano-topography to study cell-nanostructure interactions.

Summary of Research:

Infrared (IR) spectroscopy is widely used to identify chemical compounds through their molecular vibration fingerprints and has recently found many applications in biological analysis. We have developed a novel technique called Metasurface-Enhanced Infrared Spectroscopy (MEIRS) to measure live cells in physiological conditions. In MEIRS, cells are grown on an array of plasmonic nanoantennas called metasurfaces. These resonant nanoantennas support plasmonic hot spots, enhancing the light-matter interaction and IR absorption. In the past, we have used MEIRS to detect spectroscopic changes in response to cellular dissociation and cholesterol depletion [1]. Our current work focuses on expanding the application of MEIRS through the integration of metasurface with multi-well cell culture chambers for high-throughput measurement, exploring the use of MEIRS to measure cellular response from chemotherapeutics, as well as combining plasmonic metasurfaces with nano-topography to study cell-nanostructure interactions.

Figure 1 shows a schematic drawing of the MEIRS measurement setup for live cells.

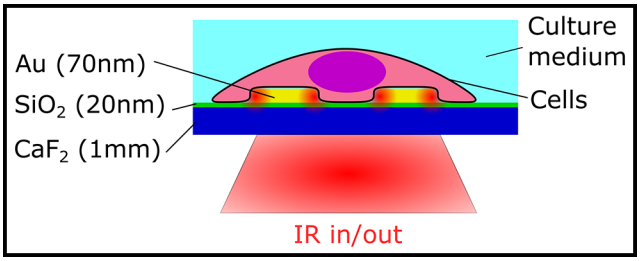

Figure 1: Schematic drawing of the metasurface-enhanced infrared spectroscopy setup for live cell measurement.

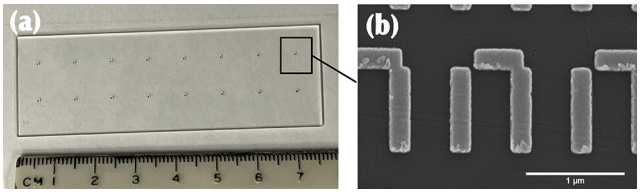

Figure 2: Metasurface integration with multi-well cell culture chamber. (a) 16 metasurface patterns fabricated on 1" × 3" CaF_2 slide, to be attached to a cell culture chamber superstructure (not shown). (b) SEM images of the metasurface. Scale bar: 1 µm.

In order to make metasurface compatible with standard cell culture in multi-well format, metasurface devices are fabricated as repeating patterns on top of a $1^2 \times 3^2$ infrared transparent CaF_2 substrate (Figure 2). The fabrication starts with a 4-inch diameter CaF_2 window, which is coated with 20 nm of SiO_2 using Oxford PECVD as a protection layer.

Metasurface patterns are defined using electron-beam lithography with the JEOL 9500 system and poly(methyl methacrylate) (PMMA) as the resist.

Then, 5 nm Cr and 70 nm Au are deposited using SC4500 evaporator. The 4-inch CaF_2 window is cut into $1^2 \times 3^2$ pieces using the DISCO dicing saw.

As the final step, Anatech or Glen 1000 Resist Strip is used to clean the metasurface sample. Commercial superstructures for multi-well cell culture chambers are attached to this metasurface for cell culture.

We used MEIRS to measure the response of live cancer cells to a novel chemotherapeutic metal complex: tricarbonyl rhenium isonitrile polypyridyl (TRIP) [2]. This drug is an endoplasmic reticulum (ER) stress inducer and regulates important biological functions such as protein synthesis. By analyzing the measured infrared spectra using linear regression, we extract the temporal changes in proteins and lipids IR absorption and local refractive index changes from the shift of metasurface plasmonic resonance. In addition, the local concentration of TRIP can be observed through its intrinsic IR absorption at the carbonyl stretching modes and is useful in monitoring the precise drug delivery time. Figure 3 shows the protein IR absorption signal of the cells in response to TRIP treatment.

We have observed an increase in protein signal in the short-term (tens of minutes) and a reduction in protein signal in the long-term (several hours). This result demonstrates that MEIRS is an effective label-free real-time cellular assay capable of detecting and interpreting the early phenotypic responses of cells to chemotherapeutics.

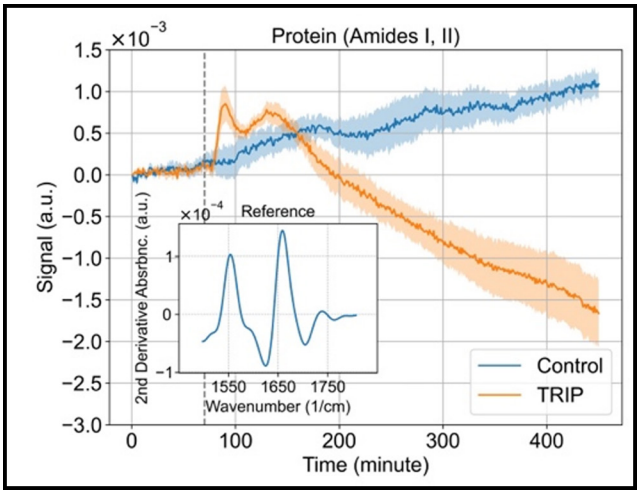

Figure 3: Cellular response to TRIP treatment. Inset: reference spectra of amide I and amide II bands attributed to proteins, used for linear regression. Dashed black line shows the timing of TRIP arrival.

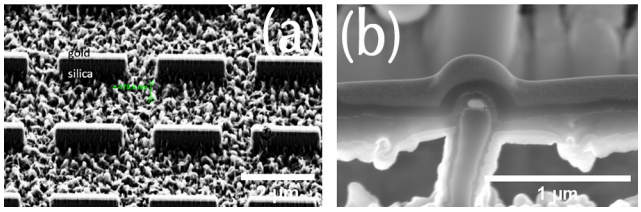

Figure 4: Nanoantenna-on-nanopillar structure. (a) SEM image of the nanoantenna-on-nanopillar structure without cells. Scale bar: 2 μm. (b) Cross section SEM image of one nanoantenna, with a cell adhered on top. Cell membrane can be seen curved around the nanoantenna-on-nanopillar. Scale bar: 1 μm.

Another direction in this project is the combination of metasurfaces with nano-topography to study cell-nanostructure interactions. Current research in surface nano-projections has shown that they can be used as effective tools to manipulate cellular attachment. We use nanopillars to incite physical and chemical responses in cells, which are then monitored through MEIRS.

We have fabricated gold nanoantennas on top of silica nanopillars (Figure 4(a)). The fabrication process starts with growing a layer of silica (~1μm) on top of CaF_2 substrate using the Oxford PECVD. Next, metasurface patterns are defined using electron-beam lithography (JEOL 9500). Gold is deposited in the patterned region using the CVC SC4500 even/odd hour evaporator. We also deposit a thin layer of chromium above the gold nanoantenna and use it as a mask to chemically etch the silica using the Plasma-Therm 740. When cells attach to such nanopillar structures, cell membrane curves around these nanopillars (Figure 4(b)), increasing the overlap between the metasurface hotspots and the cells and also increasing the concentration of certain proteins (actin, clathrin) in the metasurface hotspots.

Spectroscopically, we have observed that IR absorption from these cells on the nano-contoured metasurfaces is enhanced and shows different spectral features compared with cells on flat metasurfaces, likely related to protein secondary structures.

References:

[1] Huang, S. H., Li, J., Fan, Z., Delgado, R. and Shvets, G. Monitoring the effects of chemical stimuli on live cells with metasurface-enhanced infrared reflection spectroscopy. Lab Chip 21, 3991-4004 (2021).

[2] Shen, P.-T., et al. Probing the Drug Dynamics of Chemotherapeutics Using Metasurface-Enhanced Infrared Reflection Spectroscopy of Live Cells. Cells 11, (2022).

Arrays of Elliptical Pillars for Optical Detection of Bacteria

CNF Project Number: 2472-16
Principal Investigator(s): Gennady Shvets
User(s): Giovanni Sartorello

Affiliation(s): School of Applied and Engineering Physics, Cornell University
Primary Source(s) of Research Funding: National Cancer Institute (award number R21 CA251052), National Institute of General Medical Sciences (award number R21 GM138947) of the National Institutes of Health
Contact: gs656@cornell.edu, gs664@cornell.edu
Primary CNF Tools Used: Oxford 100 PECVD, JEOL JBX 9500FS, Oxford Cobra ICP Etcher

Abstract:

We fabricate prototype arrays of amorphous silicon nanopillars to be used for sensing bacterial binding.

Summary of Research:

Metasurfaces have been widely used for biosensing applications [1]. Organic matter, from proteins to cells, interacts with metasurfaces and changes their optical behavior, allowing detection by one of several optical techniques. In our case, we aim to use arrays of elliptical amorphous silicon nanopillars, spaced 1.2 μm in both directions, 1.2 μm tall, and in various sizes around 0.7 μm times 0.5 μm for the elliptical axes. They are intended to be used in immersion, with bacteria adhering to them. When the metasurface is illuminated in transmittance, there is a change in birefringence induced by the presence of the bound bacteria, allowing for their detection and localization.

We fabricated a prototype array by coating a glass wafer with amorphous silicon on the Oxford PECVD tool, followed by coating with a negative resist (HSQ) and EBL exposure on the JEOL 9500. After development, we used the Oxford Cobra etcher to transfer the pattern to the silicon. Timing the etching correctly was critical, because there is limited selectivity for silicon etching when using HSQ as the mask, requiring a rate measurement about midway through. Our arrays (Figure 1) match the design specifications.

Conclusions and Future Steps:

Fabrication was successful, proving the usefulness of HSQ as etching mask even with structures with relatively high aspect ratios, if etching is carefully monitored. The sample turned out not to work as hoped in the wavelength range of interest, but this can be fixed by tweaking the dimensional parameters of the metasurface. This procedure can also be applied to other devices, suited to this and many other detection techniques, by changing the design and/or materials of the metasurface.

References:

[1] Zhang, S., Wong, C. L., Zeng, S., Bi, R., Tai, K., Dholakia, K., and Olivo, M. (2021). Metasurfaces for biomedical applications: Imaging and sensing from a nanophotonics perspective. Frontiers in Optics and Photonics, 10(1), 265-299. https://doi.org/10.1515/9783110710687-023.

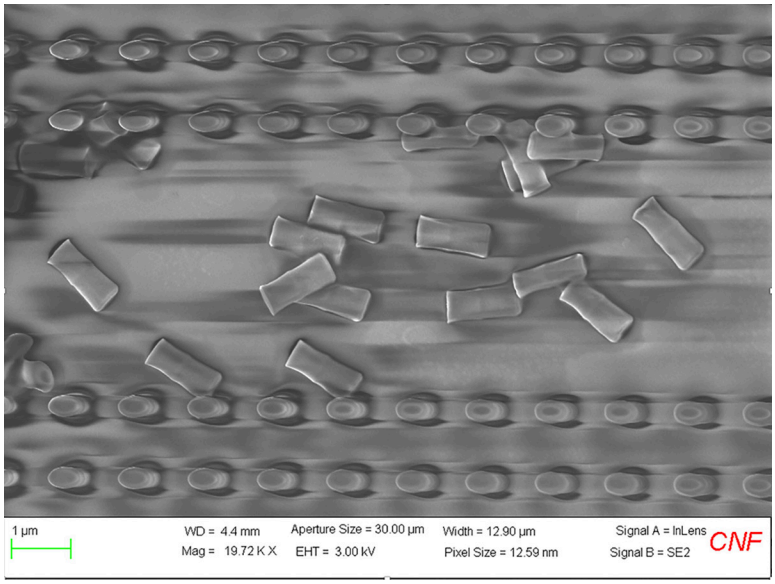

Figure 1: SEM image of one of the fabricated arrays. The pillars stand and are seen from above, except for those in the middle, which have been knocked down by the profilometer, which allows their height to be measured and shows a slight enlargement where the etching was interrupted for the rate measurement.

Studying Viral Binding and Fusion Mechanisms with Host Cell Membranes

CNF Project Number: 2575-17
Principal Investigator(s): Susan Daniel
User(s): Ambika Pachaury, Annie Chien

Affiliation(s): Smith School of Chemical and Biomolecular Engineering, Cornell University
Primary Source(s) of Research Funding: National Science Foundation, National Institutes of Health
Contact: sd386@cornell.edu, ap2387@cornell.edu, yc2499@cornell.edu
Primary CNF Tools Used: Malvern NS300 NanoSight

Abstract:

The current COVID-19 pandemic caused by the SARS-CoV-2 virus led to millions of deaths worldwide [1]. This virus is not the first of its kind; the SARS and MERS outbreaks in 2003 and 2012, respectively, were also caused by coronaviruses [1]. Additionally, the flu that we experience every year caused by the influenza virus continues to spread and we have yet to come up with a permanent solution for this viral infection [2]. Given the continuing threat these viruses pose to human health, our lab is focused on understanding the mechanisms of viral entry to determine antiviral targets. One such target is the viral fusion mechanism mediated by the spike protein in the case of coronaviruses and hemagglutinin (HA) in the case of influenza virus [1,2]. By fluorescently labelling these viruses or pseudoparticles, safer surrogates to live virus particles, we can study how they fuse with synthetic liposomes that contain receptors for the spike and HA proteins [3]. Additionally, the Daniel lab uses a chemical method to make blebs or vesicles that bud off cell membranes and can better mimic the cell membrane composition and be used for such fusion experiments [4]. These methods and experiments will provide a fundamental understanding of these viral entry events that in turn will enable us to be better prepared for future pandemics.

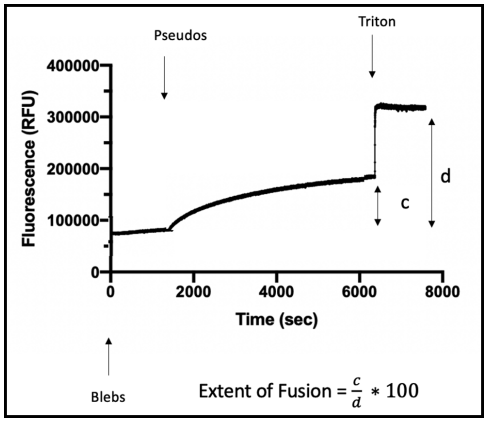

Summary of Research:

In order to test fusion between virus or viral like pseudoparticles with liposomes or cell membrane blebs, we use a method known as Ensemble Fluorescence Assay or bulk fusion assay. We label the membrane of either virus or host-cell mimic with a lipophilic dye that is self-quenched at high concentrations and then dequenches once fusion occurs. This helps us measure the extent of fusion when all the fluorescent dye is released on adding a detergent. However, in order to optimize the ratio between virus and membrane-mimic particles we rely heaving on dynamic light scattering and the NanoSight, which gives us information regarding the size, homogeneity and concentration of these particles. This concentration is critical in ensuring that we are able to get the best possible fluorescence signal and measure fusion events.

References:

[1] Tang T, Bidon M, Jaimes JA, Whittaker GR, Daniel S. Coronavirus membrane fusion mechanism offers a potential target for antiviral development. Antiviral Res. 2020 Jun;178:104792. doi: 10.1016/j.antiviral.2020.104792. Epub 2020 Apr 6. PMID: 32272173; PMCID: PMC7194977.

[2] Sriwilaijaroen N, Suzuki Y. Molecular basis of the structure and function of H1 hemagglutinin of influenza virus. Proc Jpn Acad Ser B Phys Biol Sci. 2012;88(6):226-49. doi: 10.2183/pjab.88.226. PMID: 22728439; PMCID: PMC3410141.

[3] Millet JK, Tang T, Nathan L, Jaimes JA, Hsu HL, Daniel S, Whittaker GR. Production of Pseudotyped Particles to Study Highly Pathogenic Coronaviruses in a Biosafety Level 2 Setting. J Vis Exp. 2019 Mar 1;(145):10.3791/59010. doi: 10.3791/59010. PMID: 30882796; PMCID: PMC6677141.

[4] M.J. Richards, C.-Y. Hsia, R.R. Singh, H. Haider, J. Kumpf, T. Kawate, and S. Daniel. Membrane Protein Mobility and Orientation Preserved in Supported Bilayers Created Directly from Cell Plasma Membrane Blebs. Langmuir 2016 32 (12), 2963-2974. DOI: 10.1021/acs.langmuir.5b03415.

Selective Single-Beam Acoustic Tweezers for Cell Manipulation

CNF Project Number: 2690-18
Principal Investigator(s): Alireza Abbaspourrad
User(s): Amir Mokhtare

Affiliation(s): Food Science and Technology, Cornell University
Primary Source(s) of Research Funding:
Contact: alireza@cornell.edu, am2964@cornell.edu
Primary CNF Tools Used: ABM Contact Aligner, Heidelberg Mask Writer - DWL2000, SC4500 Even-Hour Evaporator

Abstract:

Structured sound waves, mechanical waves carrying energy and momentum flux, are frontiers in advancing our understanding of cell mechanobiology. The acoustical tweezers enable biocamplatical, contact and label free manipulation of single cells and microorganisms. Focused sound beams can exert acoustic radiation force and torque that can be used for mechanical property probing and mechanosensitive ion channel activation at powers much lower than their optical counterpart. The external actuation of the mechanosensitive ion channel can act as switches for manipulation of specific cell activities in an electrical-to-chemical mediator manner.

Summary of Research:

We developed a vortex-based acoustic tweezer that can be operated from a single transparent piezoelectric transducer and can be fully integrated to a standard microscopy environment [1,2].

These vortices-based tweezers enable spatially selective manipulation of cells at single cell resolution. Furthermore, we have also developed and fabricated conventional ultrasound focusing lenses but on transparent transducers that are also easily integrated on top of the microscope objective to monitor the sound effects on biological cells [3]. (Figure 1)

To examine the feasibility of vortex-based and focused acoustic tweezers, we have built a fully integrated acoustic tweezer platform on a Nikon Ti microscope (Figure 2) and successfully performed single cell manipulation, positioning (Figure 4) and characterized it in terms of cell viability and exerted force (Figure 3). Figure 4.a shows the capability of the device in manipulating a single 7-micron diameter particle inside a microfluidic device. Figure 4.b shows the selective manipulation of a 15 μm particle using an acoustic tweezer in a microfluidic chamber observed through a standard microscope. As shown, the selected particle marked with a red circle is moved among the other particles marked in yellow, blue and green which do not move. And Figure 4.c is a representation of single budding yeast manipulation and rotation over the course of 0.3 seconds.

Conclusions and Future Steps:

Single beam acoustic tweezers that operate at biomedical ultrasound frequencies have the potential to be integrated into current conventional optical setups. Such level of integration significantly alleviates the tedious single cell manipulation procedures and lets young researchers work more efficiently on analyzing data instead of mastering working with complicated tools. It is also important to study and understand the new mechanotransduction pathways, cell reaction to stress, stress communication between cells, electromagnetic radiation consequences of mechanical stimuli, among many others that these new techniques make possible.

For the future steps, our hypothesis is that, by engineering a reliable mechanotransduction pathway that is responsible for actuating a specific signal pathway, we will be able to realize an efficient non-invasive and remote interface for on demand communication with biological entities at cellular level. Engineering focalized structured sound waves and sensitive impedance measuring sensors are the key technologies for a reversible mechanotransduction based interface between cell and electronics.

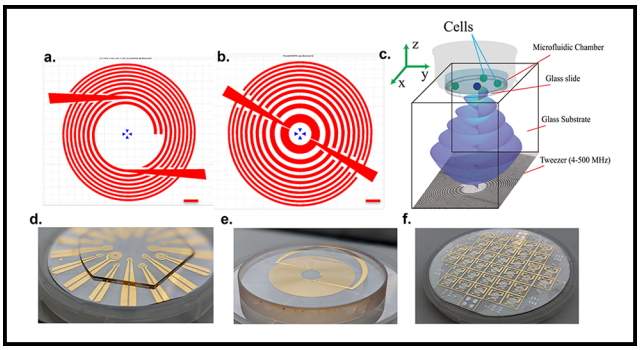

Figure 1: The acoustic tweezer and lens design. a. The intertwined spiral electrode pattern obtained from the approximate equations for frequency of 100 MHz and focal distance of 1235 µm. b. The Fresnel pattern of electrodes for acoustic focusing for f = 100 MHz and focal length of 1000 µm. Scale bar is 50 µm. c. The schematic showing the composition of the acoustic tweezer. The electrode patterns on the active piezo substrate creates a spherical vortex that propagates into the glass medium and focalizes it before it reaches the cover glass and PDMS chamber that holds the cells. The fluidic chamber on top of the acoustic tweezers is held in place by applying silicone oil as a coupler. d-f. Representative images of acoustic tweezers for manipulation of eukaryotic cells at ~ 50 MHz, embryonic female cells at ~ 5 MHz and yeast cells at ~ 200 MHz frequency.

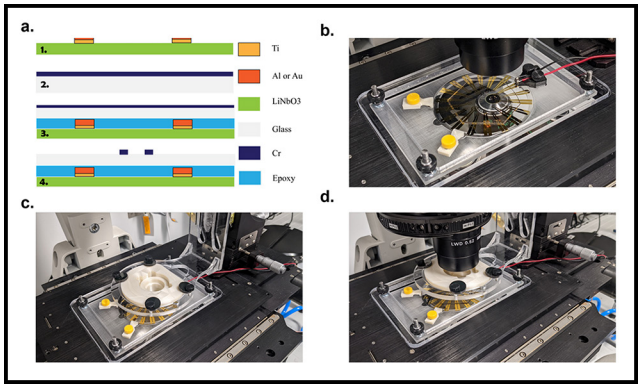

Figure 2: Acoustix tweezer fabrication and integration. a. Shows the fabrication steps. b-d. Shows the integration of the acoustic tweezer to a Nikon TE-300 microscope and 3D manipulator position that controls the fluidic chamber.

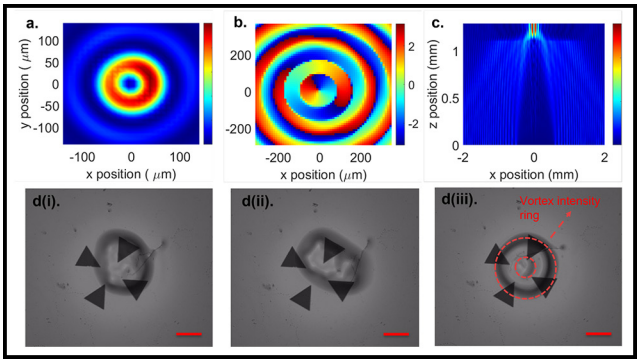

Figure 3: Numerical simulation and experimental observations. a. Intensity and b. phase prediction using angular spectrum method in the xy plane. c. intensity prediction using angular spectrum method in the xz plane. d(i)-(iii) observation of intensity profile variation during a frequency sweep to identify the acoustic tweezer resonant frequency. Scale bar is 40 µm.

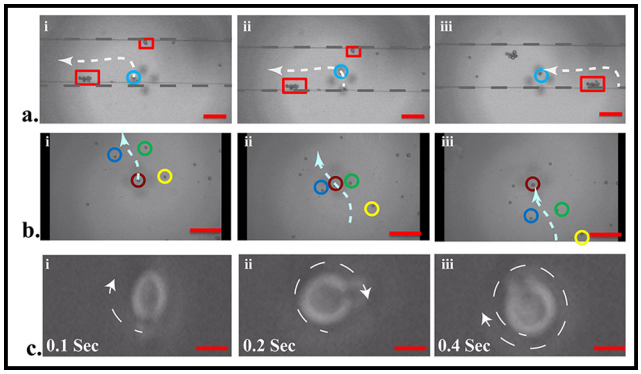

Figure 4: a. Selective manipulation of a 7 µm particle inside a microfluidic device. b. Isolation and manipulation of a 15 µm particle inside a microfluidic chamber. c. Single yeast manipulation and rotation in a microfluidic channel.

References:

[1] M. Baudoin, J.-C. Gerbedoen, A. Riaud, O. B. Matar, N. Smagin and J.-L. Thomas, Sci Adv, 2019, 5, eaav1967.

[2] M. Baudoin, J.-L. Thomas, R. A. Sahely, J.-C. Gerbedoen, Z. Gong, A. Sivery, O. B. Matar, N. Smagin, P. Favreau and A. Vlandas, Nat. Commun., 2020, 11, 4244.

[3] P. S. Balasubramanian, A. Singh, C. Xu and A. Lal, Sci. Rep., 2020, 10, 3075.

Engineering Surfaces to Investigate Cell-Material Interactions

CNF Project Number: 2748-18
Principal Investigator(s): Dacheng Ren
User(s): Yikang Xu

Affiliation(s): Biochemical and Chemical Engineering, Syracuse University
Primary Source(s) of Research Funding: National Institutes of Health
Contact: dren@syr.edu, yxu138@syr.edu
Website: https://renlab.syr.edu/
Primary CNF Tools Used: Heidelberg Mask Writer - DWL2000, ABM High Resolution Mask Aligner, Hamatech-Steag Wafer Processors, Hamatech-Steag HMP900 Mask Processing System, Unaxis SLR 770 Etcher, SC4500 Cryopumped Evaporator, DISCO Dicing Saw, MVD-100 Molecular Vapor Deposition System, Westbond 7400A Ultrasonic Wire Bonder

Abstract:

Microscale fabrication technique was employed to create master wafers for polydimethylsiloxane devices including microfluidic devices, micropillar arrays, and micro patterning. These devices were used to study bacterial response to active topography with micropillar arrays loaded with magnetic nanoparticles. The microfluidic devices were used to construct a model to simulate protein aggregation in kidney arterioles that is superior to traditional models. A valid protocol to produce a Giant Magnetoimpedance (GMI) sensor was also explored. Several iterations of the protocol were performed to troubleshoot and find a valid protocol. These platforms are useful for understanding the mechanism of cell-material interactions and complex biological processes.

Summary of Research:

Several fluid transport microfluidic devices with smallest feature size of 20 μm were fabricated by writing patterns onto masks with 1 to 1 feature ratio. The patterns were then transferred onto wafers by contact aligning and exposing photoresist coated silicon wafers, which were subsequently etched to create master wafers for soft lithography peel off process. The final microfluidic devices have channels from tens of microns to as large as millimeters in diameter mimicking capillary structure in typical human kidney vascular system. The implementation of microfluidic devices eliminates air liquid interface and intense fluidic shear force present in current laboratory protein aggregation protocols, which involves aggressive stirring of protein solution by magnetic stir bar in beakers.

Micropillar array has also been fabricated according to previously published protocol [1], where briefly, patterns of different sizes and spacing between patterns were exposed onto silicon wafer with photoresist, and etched to create high aspect ratio pillars (50:1) micro hole arrays with hole diameter as small as 2 μm. The master wafer was then used in soft lithography to create micropillar arrays with magnetic nanoparticle loaded polydimethylsiloxane. The pillars are finally placed under actuated magnetic field at different field densities for either biofilm removal or biofilm formation prevention.

A protocol for the fabrication of a GMI sensor is currently under development. This sensor consists of a sandwich structure with multiple sub-micron thick metal layers on a fused-silica wafer. The thin films were deposited with electron beam deposition and exposed several times using different masks to create three layers of different patterns on top of the substrate. A final lift-off process was done to remove photoresist and preserve the sensor structure. This sensor can be used to study cell-material interactions.

Conclusions and Future Steps:

Both microfluidic device and micropillar array master wafers were successfully fabricated with desired polydimethylsiloxane structures and excellent performance in experimental setups. For the micropillar arrays, the 50:1 aspect ratio pillar was fully achieved

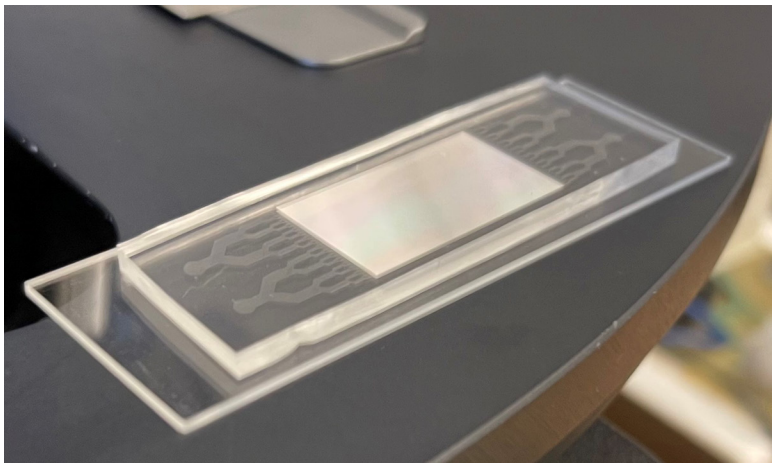

Figure 1: A picture of a microfluidic device plasma bonded to glass slide, with the channels visualized by artificial red dye.

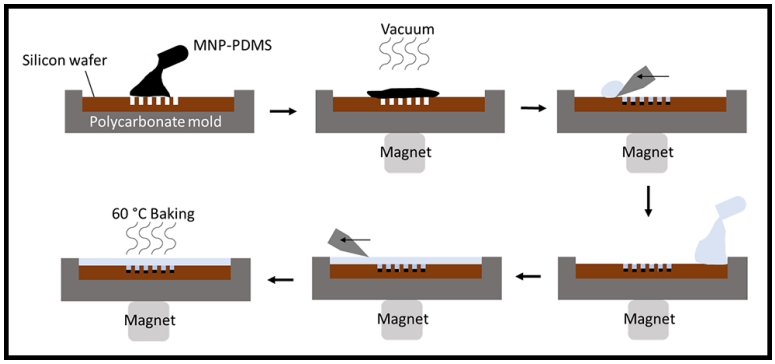

Figure 2: Illustration of fabrication process for micropillar array loaded with magnetic nanoparticles, using the master wafers.

even at the theoretical lower limit of soft lithography process (2 μm features). Future plan for these devices includes varying the dimensions or design, as well as fabricating extra master wafers for higher throughput device fabrication.

For the GMI sensor protocol, several challenges were met in the lift-off process, where the edge of the metal layers have a tendency to peel off when stripping the photoresist, resulting in partially incomplete or completely destroyed patterns. The future plan for this protocol includes optimization of pattern design to protect the layers.

References:

[1] Gu, H.; Lee, S. W.; Carnicelli, J.; Zhang, T.; Ren, D., Magnetically driven active topography for long-term biofilm control. Nature Communications 2020, 11 (1), 2211.

Fabrication of Microchip Devices for Organ-on-a-Chip and Lab-on-a-Chip

CNF Project Number: 2857-19
Principal Investigator(s): Esak (Isaac) Lee, Ph.D.
User(s): Renhao Lu, Yansong Peng

Affiliation(s): Meinig School of Biomedical Engineering, Cornell University
Primary Source(s) of Research Funding:
Contact: el767@cornell.edu, rl839@cornell.edu, yp255@cornell.edu
Primary CNF Tools Used: Heidelberg Mask Writer - DWL2000, ABM Contact Aligner, MVD 100

Abstract:

Organ-on-a-chip is a microfluidic cell culture platform, integrated circuit (chip) that simulates the activities, mechanics, and physiological response of an entire organ or an organ system. Our lab aims to create organ-on-a-chip devices to study the mechanism of various diseases. In the past year, we mainly focused on two projects: glaucoma-on-a-chip study and Micropatterned traction force microscopy for blood and lymphatic endothelial monolayer in pancreatic ductal adenocarcinoma (PDAC).

Summary of Research, Project 1: Glaucoma-on-a-Chip Model

Fluid homeostasis in the human eyes is maintained by the eye-specific fluid drainage system comprised of Trabecular meshwork (TM) and Schlemm's canal (SC). Structural and functional defects in TM and SC may impede ocular fluid drainage, elevating intraocular pressure (IOP) and damaging retinal ganglion cells, which initiates glaucoma pathogenesis. Here, we developed a dual-layer microfluidic chip system that allows coculture of TM and SC cells, recreating a three-dimensional (3D) SC channel surrounded by TM cells, mimicking the eye-specific fluid drainage system.

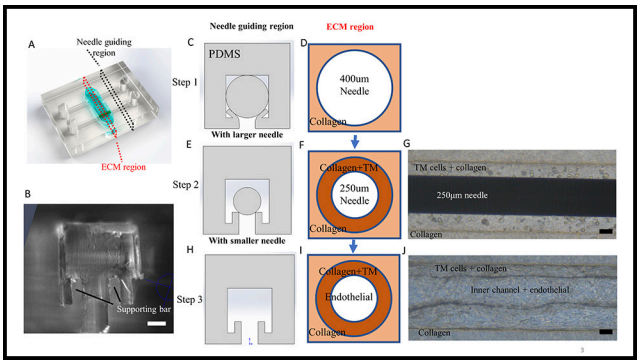

Figure 1: Fabrication of the glaucoma-on-a-chip model. (A) Schematic image of the microfluidic device. (B) The cross-section of the needle guiding region. (C-G) Three steps for fabricating the dual layer structure of TM cells and SC endothelial cells. Scale bar: (B, G, J) 50 μm.

The glaucoma-on-a-chip device design is shown in Figure 1A. In order to achieve the bilayer structure, we designed the cross-section of the needle guiding region as Figure 1B, and the function of this needle guiding region is shown in Figure 1C-J. In the first step, the larger needle was inserted into the needle guiding region, bending the supporting bar, and creating a larger cylinder channel in the ECM region (Figure 1C, D). In the second step, we filled the channel with TM cells suspended in collagen solution and inserted a smaller needle. The supporting bar kept standing to keep the smaller needle in the center of the larger channel (Figure 1E-G). In the last step, the smaller needle was withdrawn and a monolayer of endothelial cells was seeded onto the inner channel, forming a dual layer of TM and SC cells (Figure 1H-J).

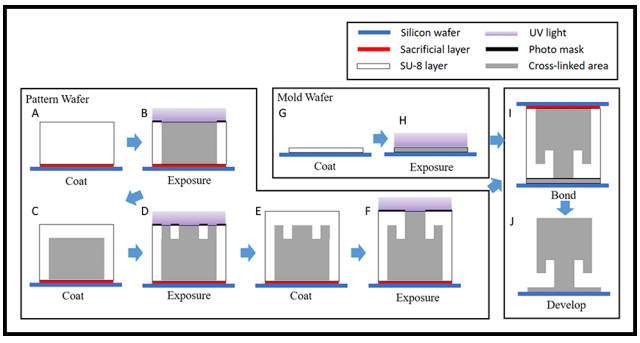

Figure 2: Modified "sandwich" method for fabricating the SU-8 needle guiding region. (A-F) One layer of OmniCoat and three layers of SU-8 were coated and exposed on the pattern wafer. (G-H) One single layer of SU-8 50 was coated and exposed on the model wafer. (I-J) The two wafers were joined before the final PEB, and the final needle guiding layer with two supporting bars was fabricated as designed.

In order to fabricate the needle guiding region with a supporting bar as shown in Figure 1B, we modified the "sandwich" fabrication method which was reported previously [1]. The microfabrication photolithography for the PDMS mold needs to combine two 100 mm

silicon wafer substrates, one was fabricated as a 'pattern wafer' (Figures 2A-F), and another was fabricated as a 'mold wafer' (Figure 2G, H).

Based on the dual layer glaucoma-on-a-chip model, we found that the coculture of SC and TM could better model the development of glaucoma compared with the monoculture of TM or SC Further, Based on NicheNet and angiogenesis reverse western arrays, we further identified VEGF-C and TGFβ as potential targets that may play a role in glaucoma development. Our finding suggests targeting VEGF-C and TGFβ pathways for the development of future glaucoma therapeutic methods.

Summary of Research, Project 2: Micropatterned TFM for Blood and Lymphatic Endothelial Monolayer in PDAC

Pancreatic ductal adenocarcinoma (PDAC) is the most common type of pancreatic cancer and one of the deadliest neoplastic malignancies in humans. It is characterized by desmoplastic stroma, paucity of tumor blood vessels, colonization of tumor-associated immunosuppressive cells, dysfunctional lymphatic vessels, and highly elevated solid stress and interstitial fluid pressure (IFP) [2]. The efficacy of immunotherapy relies on the infiltration of T cells in the tumor microenvironment (TME), but T cell infiltration is difficult under high IFP and with dysfunctional vasculature [3,4].

By combining anti-angiogenic therapy to normalize blood vessels with checkpoint blockade therapy targeting PD-L1, many mechanisms have been described for blood vascular normalization enhancement of immunotherapy in mouse tumor models [5-7]. More recent reports indicate that lymphatic vessels may play an equally significant role in the efficacy of cancer immunotherapies, previously overshadowed by harmful metastasis [8,9].

As a result of these recent findings, lymphatic vessels are now being investigated as targets to alter the TME and response to immunotherapy.

In order to understand the correlation among the intratumoral IFP, blood vessels, and lymphatic vessels, we need to investigate the relationship between vascular endothelial cadherin (VE-cad) junction and biophysical properties (i.e., traction force, intercellular force, and permeability) of endothelium with or without tumor. By creating a patterned endothelial cell monolayer on a force sensing platform, we were able to quantify and characterize the traction and intercellular force of endothelial cells in a control or tumor condition.

A microstamp mimicking the cannula shape of a vessel was fabricated using the soft lithography method (Figure 3A). The surface of a polyacrylamide gel (PAG) based substrate was preprocessed and stamped with cell adhesion molecules (e.g., fibronectin) for cell attachment (Figure 3B). Traction maps were then generated by measuring the displacement of the microbeads embedded in the gel substrate using fluorescent microscopy and Matlab processing (Figure 3C). Results were shown in Figure 4.

References:

[1] Kwak, T.J., and E. Lee. Biofabrication 13.1 (2020): 015002

[2] Osuna de la Pena, D., et al., Nat Commun, 2021. 12(1): p. 5623.

[3] Bellone, M. and A. Calcinotto, Frontiers in Oncology, 2013. 3(231).

[4] Huang, Y., et al., Nature Reviews Immunology, 2018. 18(3): p. 195-203.

[5] Mpekris, F., et al., Proceedings of the National Academy of Sciences, 2020. 117(7): p. 3728-3737.

[6] Shigeta, K., et al., Hepatology, 2020. 71(4): p. 1247-1261.

[7] Huang, Y., et al., Proceedings of the National Academy of Sciences, 2012. 109(43): p. 17561.

[8] Lund, A.W., Trends in Cancer, 2016. 2(10): p. 548-551.

[9] Vaahtomeri, K. and K. Alitalo, Cancer Res, 2020.

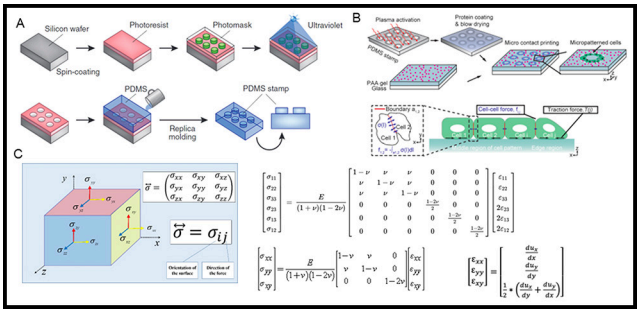

Figure 3: Schematic for micropatterned TFM. (A) Microfabrication process of PDMS stamps for micro-contact printing. Adapted from Bhatia et al., Nat. Biotech., 2014. (B) Fabrication of polyacrylamide gel based substrates with embedded fluorescent microbeads for force detection. (C) Computational modeling of traction force between the cell and the force detection substrate. (B) and (C) are both adapted from Cui, et al., Biophysical Jour., 2020.

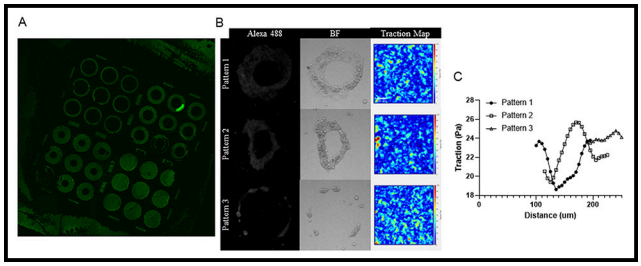

Figure 4: Micropatterned TFM for cancer cell mechanophenotyping. (A) Micropatterned surface of the force detection substrate. (B) Traction map of patterned cancer cells generated from the force detection substrate. (C) Quantification of the traction force in (B).

Human MSCs Release Multiple EV Populations Containing Mitochondria

CNF Project Number: 2864-20
Principal Investigator(s): Dr. Michelle L. Delco, DVM, PhD, DACVS
User(s): Matthew Thomas

Affiliation(s): College of Veterinary Medicine, Department of Clinical Sciences; Cornell University
Primary Source(s) of Research Funding: Harry M. Zweig Fund for Equine Research National Institute of Health-National Institute of Arthritis and Musculoskeletal and Skin Diseases
Contact: mld12@cornell.edu, mt826@cornell.edu
Primary CNF Tools Used: Malvern Nano ZS Zetasizer, Malvern NS300 NanoSight

Abstract:

A growing body of evidence supports intracellular mitochondrial (MT) transfer as an important intercellular signaling mechanism. Further, increasing evidence suggests that Mesenchymal Stromal Cells (MSCs) can rescue injured and dysfunctional cells by donating whole mitochondria, and this phenomenon may explain the beneficial effects of therapeutically implanted MSCs. One possible mechanism for MT transfer involves packaging mitochondria into extracellular vesicles (EVs). This would open the possibility of cell-free MT-targeted regenerative therapies. Confirming that this is possible would be an important step toward therapeutic development. As demonstrated here, human MSCs produce EVs containing MT. We have used the CNF facilities to further characterize these 'mitovesicles' and found that there are multiple populations of different sizes, indicating different modes of biogenesis and/or distinct bio-signaling functions.

Summary of Research:

The phenomenon of intercellular mitochondrial transfer, by which mesenchymal stromal cells donate whole mitochondria (MT) to other cell types undergoing MT dysfunction, is a promising avenue for therapeutic intervention in degenerative disease [1]. Mitochondrial donation has been demonstrated in multiple cell types, including neurons and myocytes. It has been shown to improve MT function and prevent apoptosis *in vitro*, as well as improve tissue repair *in vivo* [2–4].

Our lab studies MSC MT donation in the context of orthopedic disease, using *in vitro* chondrocyte cultures and explanted cartilage tissue as models. Using confocal imaging, we have identified several possible modes of MSC-chondrocyte MT transfer, including direct cell-cell contact (e.g., nanotubule-medial filipodial transfer, gap junction-mediated transfer) and what appears to be non-contact transfer, whereby MSCs release mitochondria into the extracellular space, which are then taken up by chondrocytes. We hypothesize that these are MT are packaged inside of extracellular vesicles (EVs) as so-called 'mitovesicles'.

This strategy of loading MT into EVs has precedent in literature. Phinney, et al., showed that MSCs can use mitovesicles, to outsource mitophagy of depolarized MT to macrophages, boosting bioenergetics for both the donating MSC and the recipient macrophage [5]. Furthermore, Morrison, et al., used cellular staining and flow cytometry to demonstrate that distressed lung epithelial cells can take up MT through EV-mediated transfer, and this ameliorates lung injury *in vivo* [6].

Our goal was to characterize the EVs produced by human MSCs. EVs are an inherently heterogenous population, making specific categorization difficult. However, it is widely recognized that they fall into three size categories: small (15-100 nm, exosomes), medium (150-1000, microvesicles), and large (1 μm+, apoptotic bodies). We isolated EVs from human bone marrow derived MSCs and used dynamic light scattering (DLS) to analyze their size distribution (Figure 1). As expected, we found the three categories supported by previous work [7] (Figure 1).

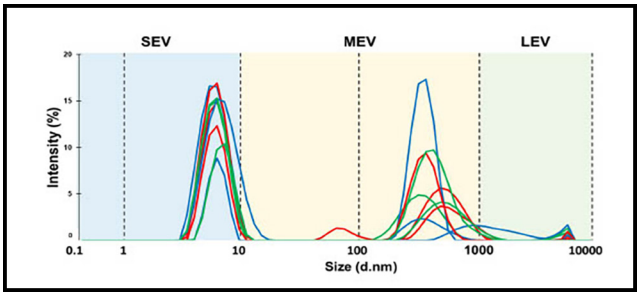

Figure 1: Dynamic Light Scattering of human MSC-derived extracellular vesicles (EVs) reveals three sub-populations of EVs based on size: small, (SEV; ~5-10nm) medium, (MEV; ~100-1000nm) and large (LEV; 5,000-10,000nm). N =3.

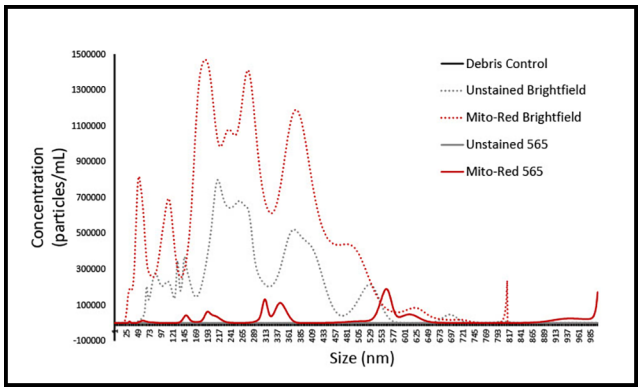

Figure 2: NTA supports trend of larger EVs containing MT. EVs were stained with Mitotracker Red and run with either a non-fluorescent (brightfield) filter, or with fluorescence exciting at 565 nm. These groups were compared to non-stained EVs and a double filtered PBS control. Unstained particles were undetectable using the 565 filter. Mitotracker positive EVs seemed to show a trend towards a larger size, with nearly all of the smallest population disappearing altogether. N = 1.

Next, we used the Malvern NS300 NanoSight to identify which, if any of these categories contain MT. We stained hMSC EVs with Mitotracker Red, then performed nanoparticle tracking analysis using the NanoSight's 565 nm fluorescent filter. We were able to validate that this method allows us to track exclusively EVs that contain mitochondrial content (Figure 2). Further, we found that mitovesicles make up around 20% of the total EV's released and appear to trend slightly larger than the general population (Figure 2). The significance of these findings is not yet clear, but likely reflects distinct modes of biogenesis and cargos for different sub-populations of mitovesicles.

Conclusions and Future Steps:

Our work thus far has confirmed our ability to isolate EVs from MSCs and identify mitovesicles within that population. Our next step is to identify and separate the EVs that contain functional and non-functional MT. This will allow us to begin identifying the role that these particles play in intercellular signaling and to further investigate MSC-EV mediated MT transfer.

This work has contributed to a poster, "MitoEVs Containing CX43 Transfer Mitochondria to Chondrocytes" that was presented at the International Gap Junction Conference 2022 and a manuscript, "Human Mesenchymal Stromal Cells Release Functional Mitochondria in Extracellular Vesicles" that is currently being proofed for publication in Frontiers in Bioengineering and Biotechnology.

References:

[1] Delco, M. L., Bonnevie, E. D., Bonassar, L. J., and Fortier, L. A. Mitochondrial dysfunction is an acute response of articular chondrocytes to mechanical injury. J. Orthop. Res. 36, (2018).

[2] Jiang, D., et al. Mitochondrial transfer of mesenchymal stem cells effectively protects corneal epithelial cells from mitochondrial damage. Cell Death Dis. 7, (2016).

[3] Konari, N., Nagaishi, K., Kikuchi, S., and Fujimiya, M. Mitochondria transfer from mesenchymal stem cells structurally and functionally repairs renal proximal tubular epithelial cells in diabetic nephropathy *in vivo*. Sci. Rep. 9, (2019).

[4] Spees, J. L., Olson, S. D., Whitney, M. J., and Prockop, D. J. Mitochondrial transfer between cells can rescue aerobic respiration. Proc. Natl. Acad. Sci. U. S. A. 103, (2006).

[5] Phinney, D. G., et al. Mesenchymal stem cells use extracellular vesicles to outsource mitophagy and shuttle microRNAs. Nat. Commun. 6, (2015).

[6] Morrison, T. J., et al. Mesenchymal stromal cells modulate macrophages in clinically relevant lung injury models by extracellular vesicle mitochondrial transfer. Am. J. Respir. Crit. Care Med. 196, (2017).

[7] Zhang, X., Hubal, M. J., and Kraus, V. B. Immune cell extracellular vesicles and their mitochondrial content decline with ageing. Immun. Ageing 17, (2020).

Scalable Continuous Flow Electroporation Platform

CNF Project Number: 2900-20
Principal Investigator(s): Thomas Corso
User(s): Jacob VanderBurgh

Affiliation(s): CyteQuest
Primary Source(s) of Research Funding: Investor funding
Contact: tcorso@cytequest.com, jvanderburgh@cytequest.com
Website: https://cytequest.com/
Primary CNF Tools Used: Odd-Hour Evaporator

Abstract:

Viral vectors are a bottleneck in the manufacturing of cell therapies. To bypass viral vectors, electroporation has emerged as a non-viral transfection method for primary cells. However, standard cuvette-style approaches are limited by difficult optimization and incompatibility with large-scale cell manufacturing. Here, we present and fabricate a novel electroporation platform that can efficiently transfect small volumes of cells for research and process optimization and scale to volumes required for applications in cellular therapy. We demonstrate of messenger ribonucleic acid (mRNA) to primary human T cells with high efficiency and viability at research scale and we demonstrate seamless scaling of delivery by increasing experimental throughput by a factor of five.

Report:

To address limitations associated with cuvette-style electroporation, CyteQuest has developed a scalable electroporation platform to optimize transfection parameters and deliver cargo efficiently and reproducibly at high throughput. Our approach incorporates a single use, continuous-flow fluidic system designed to integrate with automated cell processing approaches.

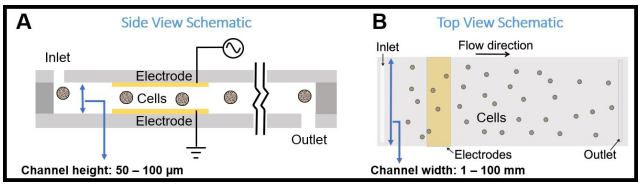

Figure 1: (A) Side view schematic of the flow cell (not to scale). (B) Top view schematic of the flow cell (not to scale).

The prototype electroporation flow cell consists of a planar flow chip with a thin slab geometry. It contains a single fluid inlet/outlet that receives cells suspended in electroporation buffer containing the cargo to be delivered. Electrodes are patterned on the top and bottom flow cell surfaces in order to apply a uniform electric field perpendicular to the flow direction (Figure 1A). The thin slab geometry of the device ensures that each cell is subject to the same electric field and the same chemical environment enabling reproducible electroporation. The shallow height (50 -100 µm) also means that we can achieve the necessary electric field strength to open pores in the cellular and nuclear membranes by applying relatively low voltages (~15 V) compared to the high voltage of traditional commercial systems. The width (1-100 mm) of the device is much larger than its depth to allow for rapid and continuous flow of the cells through the chip (Figure 1B). Importantly, the width of the device can be varied to match the desired experimental throughput without changing the electric field experienced by the cells. As such, our planar geometry enables us to seamlessly scale from small volumes of precious sample to determine optimal transfection parameters to large volumes for delivery at clinical scales.

Electroporation flow chips are constructed from a three-layer stack of polymer substrates. All three layers are laser cut with a small beam spot, high resolution carbon dioxide laser. The top and bottom layers, cut from 1 mm thick acrylic slabs, create the floor and sealing channel

surfaces. The middle layer is a spacer that defines the channel depth and width and is composed of a thin pressure sensitive adhesive tape. To fabricate the chip, the bottom and top acrylic layers are laser-cut into 1" × 2" pieces. The pieces are then laser-cut to add fluid inlet/outlet ports and alignment holes for use during the assembly process. Afterwards, a thin film electrode of gold is deposited by physical vapor deposition on the inside surface of each acrylic piece at the CNF using the odd-hour evaporator. The middle layer is cut to shape and also receives the corresponding alignment holes via the laser cutting process. The three-piece (acrylic, spacer, acrylic) sandwich assembly is then compression bonded in a press.

Cells with the cargo to be transfected are loaded into a syringe and injected through tubing into the flow cell by a syringe pump. As cells flow through the electrode pair, they experience a spatially uniform electrical field produced by a computer-controlled function generator and amplifier. The applied voltage waveform and resultant current are monitored via an oscilloscope. The electroporated cells then exit the flow cell and are dispensed into wells of a well-plate by a robotic fraction collector. Computer-controlled waveform selection and robotic sampling enable rapid sweeping of waveform parameters such as the voltage amplitude or waveform shape.

Using this system, CyteQuest has delivered mRNA encoding green fluorescent protein (GFP) to primary human T cells with high efficiency and high viability, observing > 95% transfection efficiency with < 2% loss of cell viability compared to control cells (Figure 2). To demonstrate the ability of our device to scale experimental throughput, we increased the width of the device from 2 to 10 mm and the volumetric flow rate from 320 µL/min to 1.6 mL/min (Figure 3A-B). Scaling both the channel width and flow rate by a factor of five produced identical GFP expression and viability values in both channel widths for Jurkat cells transfected with mRNA encoding GFP (Figure 3B). Overall, these data demonstrate the ability of our platform to efficiently deliver mRNA to cells and seamlessly scale-up delivery without changing delivery performance.

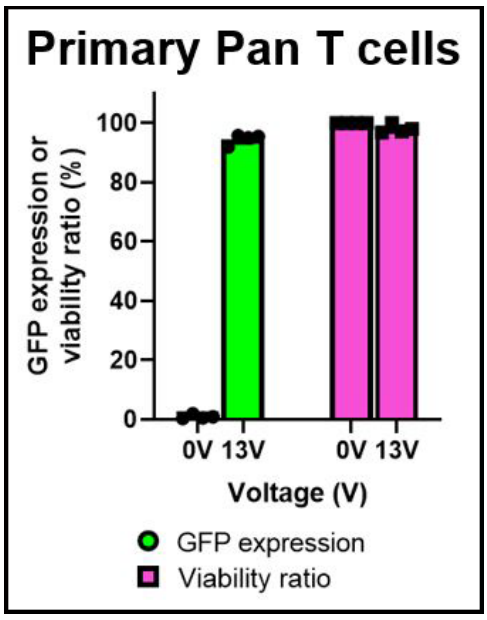

Figure 2: Delivery of mRNA to primary human T cells. Data from primary T cells from four healthy donors (n = 4). Data shown as mean ± standard deviation.

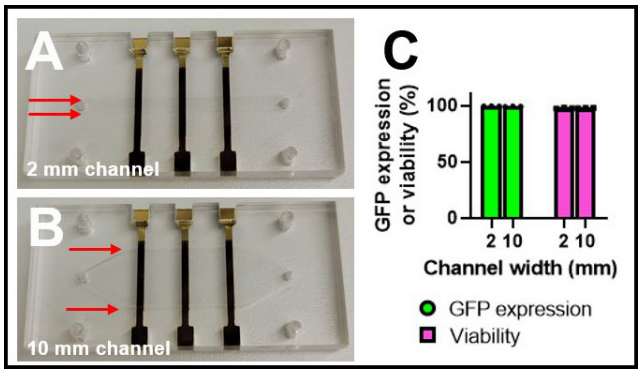

Figure 3: Scaled-up delivery of mRNA to Jurkat cells. (A) Photograph of a 2 mm and (B) 10 mm electroporation flow cell. Red arrows highlight the channel width. (C) Plot of GFP expression and viability values from Jurkat cells transfected with mRNA encoding GFP in either the 2- or 10-mm channels (n = 3). Data shown as mean ± standard deviation.

Plant Membrane Bioelectronic Devices for the Study of a Membrane Transporter

CNF Project Number: 2908-20
Principal Investigator(s): Susan Daniel
User(s): Barituziga Banuna, Miriam Huerta

Affiliation(s): Smith School of Chemical and Biomolecular Engineering, Cornell University
Primary Source(s) of Research Funding: NSF EAGER GRANT
Contact: sd386@cornell.edu, bb675@cornell.edu, gh437@cornell.edu
Primary CNF Tools Used: Malvern NS300 NanoSight

Abstract:

As a "label-free" alternative to optical sensing, electrical sensing represents a more feasible, reproducible, and scalable detection method [1,2]. Among various electrical sensing techniques, the non-invasive electrochemical impedance spectroscopy (EIS) technique is especially suitable for accurately quantifying the bio-recognition events occurring at a variety of biointerfaces, such as bacterial, viral, cellular and synthetic lipid membranes [3,4]. Our group aims to design a microelectrode system that will support the self-assemble of supported lipid bilayers (SLBs) on the electrode surfaces, and their electrical properties (resistance, capacitance) can be extracted by applying an alternating voltage and recording the current response [4-7]. Since the electrode dimensions and the local environment are readily controlled via photolithography, this system gives us a edge to easily mimic and manipulate the local environment to support the assembly of various SLBs of interest. Future work will focus on the incorporation of the microfluidic system into the microelectrode system.

Summary of Research:

Lipid vesicle nanoparticles were induced to form via chemical induction of cell-wall free Arabidopsis Thaliana plant protoplast. These vesicles or blebs composed of the native membrane materials were collected and then the size, distribution and concentration were characterized via NTA with Malvern NS300 NanoSight. Following characterization, blebs were used to form SLBs on microelectrodes and the resulting device was used with electrical sensing techniques such as EIS.

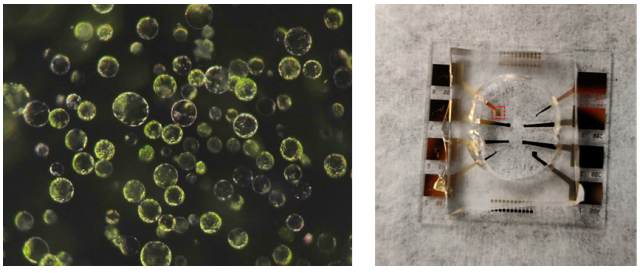

Figure 1: Arabidopsis Thaliana *derived protoplast (left); PDMS well stamped on a single device to enable self-assembling of SLB and EIS measurement (right).*

References:

[1] Berggren, Magnus, and Agneta Richter-Dahlfors. "Organic bioelectronics." Advanced Materials 19.20 (2007): 3201-3213.

[2] Chalklen, Thomas, Qingshen Jing, and Sohini Kar-Narayan. "Biosensors based on mechanical and electrical detection techniques." Sensors 20.19 (2020): 5605.

[3] Magar, Hend S., Rabeay YA Hassan, and Ashok Mulchandani. "Electrochemical Impedance Spectroscopy (EIS): Principles, Construction, and Biosensing Applications." Sensors 21.19 (2021): 6578.

[4] Lisdat, F., and D. Schäfer. "The use of electrochemical impedance spectroscopy for biosensing." Analytical and Bioanalytical Chemistry 391.5 (2008): 1555-1567.

[5] Tang, Tiffany, et al. "Functional infectious nanoparticle detector: Finding viruses by detecting their host entry functions using organic bioelectronic devices." ACS Nano 15.11 (2021): 18142-18152.

[6] Bint E Naser, Samavi Farnush, et al. "Detection of Ganglioside-Specific Toxin Binding with Biomembrane-Based Bioelectronic Sensors." ACS Applied Bio Materials 4.11 (2021): 7942-7950.

[7] Pappa, Anna-Maria, et al. "Optical and electronic ion channel monitoring from native human membranes." ACS Nano 14.10 (2020): 12538-12545.

Investigating the Effect of the Tumor Microenvironment on Metastatic Progression using Micro and Nano-Scale Tools

CNF Project Number: 2912-20

Principal Investigator(s): Claudia Fischbach

User(s): Matthew Tan, Niaa Jenkins-Johnston, Nicole Sempertegui

Affiliation(s): Biomedical Engineering, Cornell University

Primary Source(s) of Research Funding: 2021 Cornell NanoScale Facility REU Program National Science Foundation Grant No. NNCI-2025233, Stem Cell Research Training Fellowship Stem Cell Program of Cornell University, the Center on the Physics of Cancer Metabolism National Cancer Institute Award Number 1U54CA210184-01

Contact: cf99@cornell.edu, mlt239@cornell.edu, noj4@cornell.edu, nds68@cornell.edu

Primary CNF Tools Used: ABM Contact Aligner, Heidelberg Mask Writer - DWL2000, Hamatech 9000, Malvern NS300 NanoSight

Abstract:

Breast cancer mortality is driven by metastasis, where cancer cells disseminate from the primary tumor to seed distant tissues. During the metastatic cascade, cancer cells interact with their microenvironment consisting of extracellular matrix including collagen and other cell types including endothelial cells in blood vessels and mesenchymal stromal cells (MSCs) in the bone. Cancer cells may interact locally or from distant sites through mechanisms such as soluble factor and extracellular vesicle (EV) signaling. In this study, CNF tools were used to investigate the two stages in metastasis: early invasion towards blood vessels and EV-mediated formation of a pre-metastatic niche. For the former, we developed a microfluidic model of the perivascular niche and found that ECs stimulate breast cancer invasion into collagen, and that an EC-coated micro channel exhibits a distinct diffusion profile from a channel without ECs. For the latter, we've been able to isolate and characterize EVs from two breast cancer cell lines. Future work will continue to use the microfluidic model to investigate the mechanisms by which ECs influence cancer invasion and apply EVs to MSCs on a bone-mimetic model system to investigate how cancer cells can influence the formation of a pre-metastatic niche.

Summary of Research:

Introduction. Breast cancer is the second leading cause of cancer-related death for women in the United States [1]. Mortality in breast cancer is driven by metastasis, where tumor cells disseminate from the primary tumor and spread to distant tissues. During this process, tumor cells become invasive and move towards blood vessels, where they will enter the circulation and seed onto distance sites such as the bones. Tumor cells that proceed through the metastatic cascade encounter a changing microenvironment consisting of extracellular matrix (ECM) such as collagen and other cell types, including endothelial cells (ECs) and mesenchymal stromal cells (MSCs) [2]. These cells are known to participate in reciprocal signaling with tumor cells to influence tumorigenesis through the exchange of soluble factors [2,3].

Incidentally, tumor cells may even be able to prime future metastatic sites through the release of extracellular vesicles (EVs) that enable long distance transport of cell-derived cargo [4]. However, the mechanisms by which soluble factor and EV signaling influence tumor cell invasion and the development of a pro-tumorigenic microenvironment remain unclear due to the lack of models that enable systematic study. To this end, we have used the expertise at the CNF to investigate two key steps in the metastatic cascade: initial invasion towards ECs in blood vessels, and EV-mediated formation of the pre-metastatic niche.

Regulation of Breast Cancer Invasion Using a Microfluidic Model of the Perivascular Niche. In early invasion, tumor cells initially invade towards blood vessels, responding to metabolic gradients from the vessels and signaling gradients from ECs. Using SU-8 photolithography in conjunction with the ABM Contact Aligner and a photomask generated by the Heidelberg DWL2000, we have created a dual-channel microfluidic devices that enables co-culture of breast cancer cells and ECs encapsulated in a 3D collagen matrix. In this system,

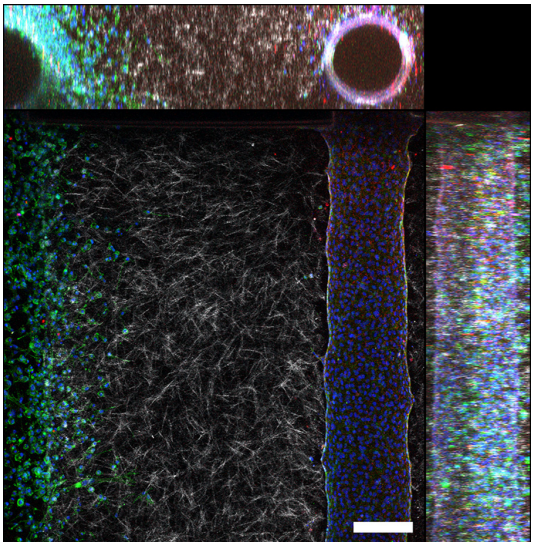

Figure 1: Confocal microscopy projection of breast cancer cells stained with invading into collagen in response to an endothelial cell channel stained with CD31 (red). DAPI was used to stain nuclei (blue), phalloidin was used to stain f-actin (green), and confocal reflectance was used to visualize collagen fibers (white). Scale bar: 200 µm.

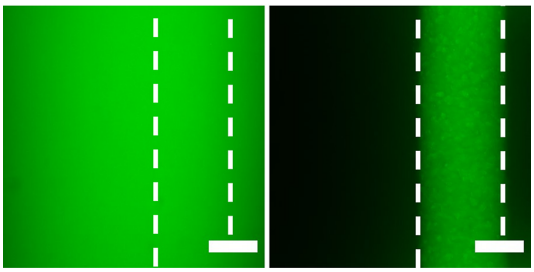

Figure 2: Diffusion of fluorescein (FITC) from a non-human umbilical vein endothelial cell (HUVEC) channel and a HUVEC coated channel. Scale bar: 200 µm.

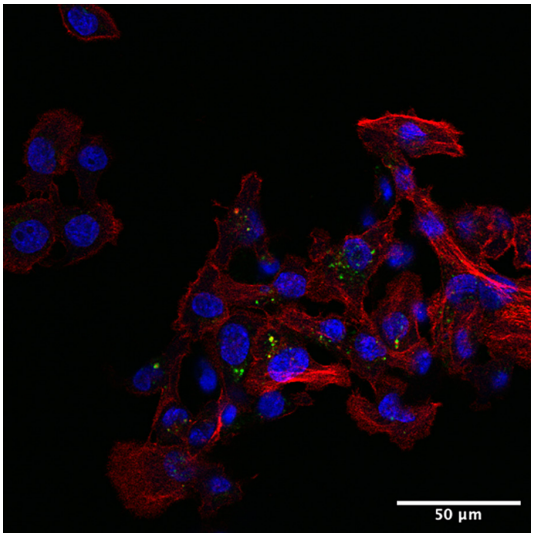

Figure 3: Extracellular vesicles labeled with a DiO lipophilic dye (green), MCF10ACA1a cells labeled with DAPI for nuclei (blue) and phalloidin for f-actin (red). Scale bar: 50 µm.

we found that the presence of ECs stimulated cancer invasion into a collagen hydrogel (Figure 1). Additionally, using fluorescent molecule diffusion studies, we found that an EC-coated channel restricted diffusion of molecules within in the channel compared to a channel without ECs (Figure 2).

Isolation and Characterization of Breast Cancer-Derived Extracellular Vesicles. Prior to arriving at distant metastatic sites, tumor cells can release soluble factors and extracellular vesicles (EVs) into the circulation to prime the microenvironment of distant target organs for subsequent development of organotropic metastasis. While soluble factor signaling plays a demonstrated role in cancer, EVs are gaining appreciation as stable vehicles of cell-derived cargo contributing to tumorigenesis and pre-metastatic niche (PMN) formation. Thus far, we have successfully isolated and characterized EVs from MDA-MB-231s and MCF10CA1a breast cancer cells using the Malvern NS300 NanoSight (Figure 3). Additionally, we have started to investigate differences in cell adhesion between MSCs cultured in the presence or absence of EVs that bind to the bone matrix.

Conclusions and Future Steps:

In this project we were able to develop tools and pipelines to study the breast cancer metastatic cascade. We were able to successfully fabricate and culture a 3D microfluidic tumor-perivascular niche model. Future work using this device will be to uncover the metabolic and mechanical mechanisms by which ECs influence breast cancer invasion. We were also able to isolate and characterize breast cancer derived ECs. Future work will assess markers of MSC behavior in the presence of EVs in a biomimetic mineralized bone scaffold. This will include investigating differences in differentiation fate, proliferation and cytokine secretion. Finally, we will examine whether these changes in MSC phenotype in turn affect metastatic breast cancer cell outgrowth.

Acknowledgements:

The work described was supported by the Center on the Physics of Cancer Metabolism through Award Number 1U54CA210184-01 from the National Cancer Institute. The content is solely the responsibility of the authors and does not necessarily represent the official views of the National Cancer Institute or the National Institutes of Health.

References:

[1] Siegel, R. L., Miller, K. D., Fuchs, H. E., and Jemal, A. Cancer Statistics, 2021. CA. Cancer J. Clin. 71, 7-33 (2021).

[2] Tan, M. L., Ling, L., and Fischbach, C. Engineering strategies to capture the biological and biophysical tumor microenvironment *in vitro*. Adv. Drug Deliv. Rev. 176, 113852 (2021).

[3] Zheng, P., and Li, W. Crosstalk Between Mesenchymal Stromal Cells and Tumor-Associated Macrophages in Gastric Cancer. Front. Oncol. 10, 1-9 (2020).

[4] Peinado, H., et al. Pre-metastatic niches: organ-specific homes for metastases. Nat. Rev. Cancer 17, 302-317 (2017).